Chemosphere 368 (2024) 143771

Contents lists available at ScienceDirect

Chemosphere

journal homepage: www.elsevier.com/locate/chemosphere

Characterization of AhR-mediated potency in sediments from Kongsfjorden, Svalbard: Application of effect-directed analysis and nontarget screening

Jiyun Gwak [a,1], Jihyun Cha [a,1], Seung-Il Nam [b], Jung-Hyun Kim [b], Junghyun Lee [c], Hyo-Bang Moon [d], Jong Seong Khim [e], Seongjin Hong [a,*]

[a] Department of Earth, Environmental & Space Sciences, Chungnam National University, Daejeon, 34134, Republic of Korea
[b] Division of Glacier and Earth Sciences, Korea Polar Research Institute, Incheon, 21990, Republic of Korea
[c] Department of Environmental Education, Kongju National University, Gongju, 32588, Republic of Korea
[d] Department of Marine Science and Convergence Engineering, Hanyang University, Ansan, 15588, Republic of Korea
[e] School of Earth and Environmental Sciences & Research Institute of Oceanography, Seoul National University, Seoul, 08826, Republic of Korea

HIGHLIGHTS

- Great AhR-mediated potency was observed in sediments around the abandoned coal mines.
- PAHs in sediments were found to originate primarily from coal and coal combustion.
- BbA and 1 MC were identified as the major AhR agonists in Kongsfjorden sediments.
- 48 AhR agonist candidates were derived through NTS; 27 were coal-derived substances.

GRAPHICAL ABSTRACT

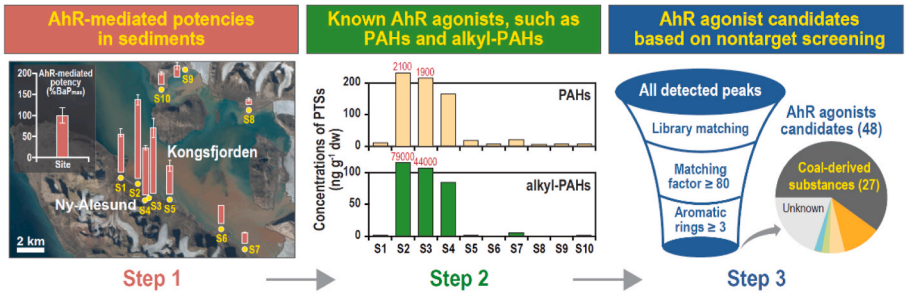

ARTICLE INFO

Keywords:
Effect-directed analysis
Nontarget screening
AhR-mediated potency
Kongsfjorden
Sediment
Coal

ABSTRACT

In this study, we aimed to identify the major aryl hydrocarbon receptor (AhR) agonists in surface sediments (S1–S10, n = 10) from Kongsfjorden, Arctic Svalbard, using effect-directed analysis. High AhR-mediated potencies were observed in the mid-polar fractions and RP-HPLC subfractions (F2.6–F2.8; log K_{OW} 5–8) in the sediments of sites S2 and S3, which are located near abandoned coal mine areas, as assessed by the H4IIE-*luc* bioassay. The concentrations of traditional polycyclic aromatic hydrocarbon (t-PAHs), emerging PAHs, alkyl-PAHs, and styrene oligomers ranged from 6.1 to 2100 ng g^{-1} dry weight (dw), 0.5–1000 ng g^{-1} dw, 47 to 79,000 ng g^{-1} dw, and 4.2–130 ng g^{-1} dw, respectively, with elevated levels in S2 and S3. Principal component analysis coupled with multiple linear regression suggested that t-PAHs in sediments primarily originated from coal, petroleum combustion, and coal combustion. Twenty-four target AhR agonists accounted for 3.2%–100% (mean = 47%) of the total AhR-mediated potencies in S2 and S3. Nontarget screening via GC-QTOFMS in the highly potent fractions identified 48 AhR agonist candidates through four-step selection criteria. Among these, 27 compounds were identified as coal-derived substances. VirtualToxLab in silico modeling predicted that most of the 48 tentative AhR agonist candidates could bind to AhR. Overall, our findings indicate significant

* Corresponding author.
E-mail address: hongseongjin@cnu.ac.kr (S. Hong).
[1] These authors contributed equally to this work.

https://doi.org/10.1016/j.chemosphere.2024.143771
Received 16 August 2024; Received in revised form 13 November 2024; Accepted 16 November 2024
Available online 23 November 2024

contamination of the Kongsfjorden sediments by coal-derived substances, highlighting the need for further studies to assess the ecological risks associated with these contaminants.

1. Introduction

Ny-Ålesund in Spitsbergen, located in the Svalbard archipelago of Norway, is one of the northernmost inhabited locations in the world, surrounded by remote areas and glaciers (Dowdall et al., 2004; Han et al., 2022; Jiao et al., 2009). The environment of Ny-Ålesund is home to a variety of plants (e.g., moss) and animals (e.g., polar bears and reindeer), as well as existing mineral resources (e.g., coal) (Dowdall et al., 2004; Han et al., 2022). Persistent toxic substances (PTSs) in various environmental media in Ny-Ålesund have a history of contamination due to long-distance transport through the atmosphere and ocean currents (Cha et al., 2024; Lee et al., 2023; Vecchiato et al., 2018). Additionally, local pollution sources such as past coal mining activities, research, and tourism have contributed to the contamination of PTSs in this area (Jiao et al., 2009). Ny-Ålesund was an active coal mining area in the early to mid-20th century (Dowdall et al., 2004). Although mining operations ceased entirely following a mining explosion, abandoned equipment and coal piles remain in the area (Dowdall et al., 2004). Ny-Ålesund functions as an international scientific base for Arctic environmental research, and local pollution from human activities continues (Jiao et al., 2009). As a result, the concentrations of PTSs in sediments from Kongsfjorden are relatively elevated compared to other fjords in Svalbard (Lin et al., 2022; Pouch et al., 2017).

Representative PTSs resulting from anthropogenic activities include polycyclic aromatic hydrocarbons (PAHs) and styrene oligomers (SOs) (Lee et al., 2022). PAHs are generated from various sources such as coal, crude oil, incomplete combustion of fossil fuels, and metal smelting (Ghosh et al., 2015). SOs are known to be produced by the thermal decomposition of polystyrene plastics (Hong et al., 2016). Some PAHs and SOs are known to act as aryl hydrocarbon receptor (AhR) agonists (Eichbaum et al., 2014). AhR mediates the toxic effects of certain toxic substances and can cause carcinogenicity and developmental toxicity in organisms (Eichbaum et al., 2014; Hong et al., 2016; Xiao et al., 2017). The assessment of AhR-mediated potencies in environmental samples has been performed using in vitro bioassay with cell lines such as H4IIE-*luc* (Cha et al., 2019; Choi et al., 2024; Gwak et al., 2022). Effect-based monitoring using in vitro bioassay can overcome the limitations of target chemical analysis, which cannot measure the mixture effects of compounds and unknown toxic substances (Neale et al., 2023). This method is expected to be useful in assessing the potential biological effects of natural and anthropogenic pollutants in the Arctic environment, but its application remains limited.

Effect-directed analysis (EDA) has been employed to identify major causative substances in complex environmental samples, such as sediments (Hashmi et al., 2018; Hong et al., 2016). EDA combines bioassays to identify active fractions, reduces sample complexity through fractionation, and determines major toxicants in the highly potent fractions via chemical analysis (Hong et al., 2023). Target chemical analysis using mass spectrometers (MS) is used to detect specific toxic substances in environmental samples with high selectivity and sensitivity (Moschet et al., 2017). However, target chemical analysis has limitations in providing comprehensive information on all the compounds in environmental samples (Masclet et al., 1986; Sim et al., 2022). To overcome this, nontarget screening (NTS) is performed using high-resolution MS (Hong et al., 2023). NTS can theoretically detect many compounds in samples without preselecting analytes or using reference standards (Bletsou et al., 2015; Masiá et al., 2014). Representative high-resolution MS systems include quadrupole time-of-flight (QTOF) MS and Orbitrap MS, which provide sensitive spectral data with high mass resolution and accurate mass values (mass error < 5 ppm) (Ccanccapa-Cartagena et al., 2019). EDA combined with NTS is a powerful tool for identifying unmonitored toxicants in samples. It has been applied to various environmental samples, such as dust (Yu et al., 2018), wastewater (Sim et al., 2022), river water (Ccanccapa-Cartagena et al., 2019), and sediments (Cha et al., 2019).

Studies identifying major toxicants in the environmental media of Arctic Svalbard have been rare to date. This study hypothesizes that sediments from Kongsfjorden are contaminated with AhR-active substances due to various human activities and that major toxicants can be identified using EDA and NTS. The specific objectives are to: i) investigate AhR-mediated potencies in sediments from Kongsfjorden, ii) determine the distribution and sources of PTSs in sediments, iii) evaluate the contribution of target AhR agonists to the total induced AhR-mediated potencies, iv) select tentative AhR agonists through NTS, and v) predict the toxicities of tentative AhR agonists using in silico modeling.

2. Materials and methods

2.1. Sample collection

In July 2022, ten surface sediments (S1–S10, n = 10) were collected from Kongsfjorden, Svalbard. In addition, coal residues (S2-1, S3-1, and S4-1) were collected from land areas near sites S2, S3, and S4 (Fig. 1a). Site S2 is historically significant as a former miners' habitation area, and remnants such as containers and equipment remain today (Fig. S1). Sites S3 and S4 are located near an abandoned mine where coal debris was also found. Furthermore, international research bases near S2 and S3 could potentially contribute to anthropogenic contaminants. The surface sediment and coal samples were stored in glass bottles, kept in an icebox, and frozen at −20 °C until laboratory analysis.

2.2. Analysis of organic carbon and total nitrogen contents

To quantify organic carbon (OC) contents, approximately 1 g of sediment was treated with 1 M HCl (Sigma-Aldrich, St. Louis, MO) to remove inorganic carbon. Following acid treatment, distilled water was added to neutralize the remaining acid, and the supernatant was removed by centrifugation. The sample was then freeze-dried. OC content was analyzed using an elemental analyzer (EA; Vario ISOTOPE cube, Elementar, Hanau, Germany). The total nitrogen (TN) content in the sediment was determined without any pretreatment (Ra et al., 2014).

2.3. Organic extraction and fractionation

The sediments were freeze-dried, sieved through a 1 mm mesh, and homogenized prior to use. Twenty grams of sediment from S1–S10 and coal samples from S2-1–S4-1 were extracted with dichloromethane (DCM, Honeywell, Charlotte, NC) using an accelerated solvent extractor (Dionex ASE 350, Thermo Scientific, Salt Lake, UT). To remove sulfur from the raw extracts (REs), activated copper was added, and the mixture was allowed to react for about 1 h. After the reaction, the REs were concentrated to a final volume of 2 mL using a rotary evaporator and a nitrogen gas concentrator. The REs were then split, with 1.5 mL allocated for silica gel fractionation and 0.5 mL reserved for bioassays. For the bioassays, the REs were solvent-exchanged to dimethyl sulfoxide (DMSO, Sigma-Aldrich).

A two-step fractionation process was performed to reduce the complexity of the samples. First, silica gel fractionation based on polarity was conducted. The REs were loaded onto a silica gel column containing 8 g of activated silica gel (Sigma-Aldrich) and eluted with 30

mL of hexane (F1, non-polar fraction), 60 mL of hexane:DCM (8:2) (F2, mid-polar fraction), and 50 mL of DCM:acetone (6:4) (F3, polar fraction). The eluted fractions were concentrated to 1.5 mL. In the second step, the 1 mL silica gel fraction was subjected to reverse-phase high-performance liquid chromatography (RP-HPLC) fractionation. Detailed RP-HPLC conditions are provided in Table S1.

2.4. H4IIE-luc in vitro bioassay

The AhR binding affinity in sediment organic extracts, silica gel fractions, and RP-HPLC fractions was measured using H4IIE-*luc* recombinant cells (Table S2). Cells were detached using trypsin, and then 250 μL of cells were dispensed into 96-well plates at a concentration of 7.0×10^4 cells mL^{-1}. The cells were incubated at 37 °C with 5% CO_2 for 24 h and then exposed to the controls, REs, and fractions. Benzo[*a*]pyrene (BaP) was used as the positive control, 0.1% DMSO as the negative control, and the culture medium as the control. The initial concentration of BaP was set at 50 nM (=100% BaP_{max}) and then diluted by 3 times, and exposed to a total of six concentrations. Luciferase luminescence was measured using a Victor X3 multilabel plate reader (PerkinElmer, Waltham, MA) after 4 h exposure. The bioassay results were converted to a percentage of the maximum BaP response. Potency-based BaP-equivalent concentrations (BaP-EQs) in the sediment subfractions were calculated from the dose-response relationship. To ensure reproducibility, all samples were tested in triplicate during the bioassay.

2.5. Target chemical analysis

Target chemical analysis was conducted for 15 traditional PAHs (t-PAHs), 14 emerging PAHs (e-PAHs), 20 alkyl-PAHs, and 10 SOs using gas chromatography (GC; Agilent 7890B, Agilent Technologies, Santa Clara, CA) coupled with a 5977B mass selective detector (MSD; Agilent Technologies). The instrumental conditions for the GC-MSD, full names of compounds, and method detection limits are provided in Tables S3 and S4. The recovery rates of surrogate standards (SS) were measured to assess any potential loss of compounds during the experimental process. Isotopically labeled SS (acenaphthene-d10, phenanthrene-d10, and chrysene-d12) were added to the procedural blank and sediment samples, and the recovery rates of the SS ranged from 67 to 105% and 70–110%, respectively.

2.6. Nontarget screening of highly potent fractions

NTS was conducted using GC-QTOFMS on RP-HPLC subfractions that exhibited high AhR-mediated potencies. The instrumental conditions for the GC-QTOFMS are provided in Table S5. Tentative AhR agonists were identified through four-step selection criteria. First, all chromatographic peaks from the sediment samples were identified (Schymanski et al., 2014). Second, these peaks were matched to compounds in the NIST library (Gwak et al., 2022). Third, compounds with a match score of 80 or higher were selected (Zedda and Zwiener, 2012). Finally, tentative AhR agonist candidates with three or more aromatic rings were identified (Cheng et al., 2024).

2.7. Potency balance analysis

Potency balance analysis was conducted by comparing instrument-derived BaP-EQs (BaP-EQ_{chem}) with bioassay-derived BaP-EQs (BaP-EQ_{bio}) for the same sample in order to assess the contribution of individual AhR agonists to the overall AhR-mediated potency. BaP-EQ_{chem} was calculated as the sum of the products of concentrations and relative potency values (RePs) for individual compounds, as reported in previous studies (details are provided in Table S6).

2.8. Principal component analysis with multiple linear regression

Principal component analysis with multiple linear regression (PCA-MLR) was conducted to identify the sources of t-PAHs in the sediments (Hopke, 2003), using the concentrations of 15 t-PAHs, excluding naphthalene (Na). The factor loading and score matrices can be derived from the t-PAH concentration dataset. This equation was adapted from a previous study (Feng et al., 2014), where X represents the PAH concentration matrix, L is the factor loading matrix, and T is the factor score matrix (Eq. (1)).

$$X = L \times T \quad \text{(Eq. 1)}$$

The factor loading matrix facilitates the identification of potential source categories, and PCA scores are derived from the factor score matrix. The contribution of each source to the total PAHs load in sediments can be quantified by applying MLR to the PCA scores. The PCA-MLR employed varimax rotation and Kaiser normalization to identify the contributing factors for PAHs. Only factors with eigenvalues of 1 or greater were considered as main components (Qishlaqi and Beiramali, 2019). To confirm the stability of the variables for PCA, the

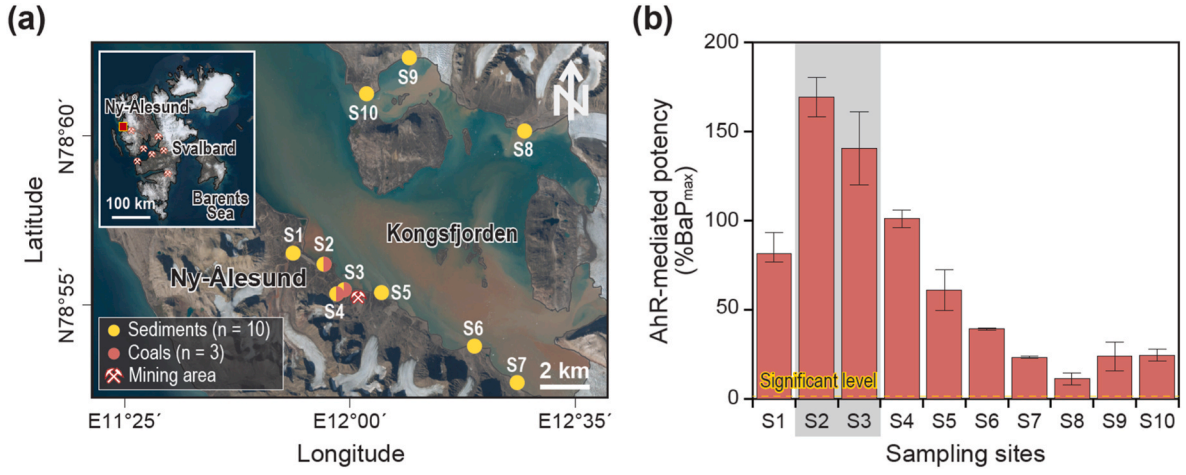

Fig. 1. (a) Map showing the sampling sites in Kongsfjorden. The samples of surface sediments (S1–S10, n = 10) and coal (S2–S4, n = 3) were collected in July 2022. **(b)** AhR-mediated potencies in raw organic extracts of sediments from Kongsfjorden The significant level was calculated by dividing the standard deviation of the RLU value of the solvent control group by the RLU value of the maximum concentration of the positive control group (Gray shade: greater AhR-mediated potencies; Error bar: mean ± standard deviation; n = 3).

Kaiser–Meyer–Olkin (KMO) test was conducted, yielding a measure exceeding 0.5, which meets the suitability criteria.

2.9. VirtualToxLab and VEGA QSARs in silico modeling

The AhR binding affinities of the AhR agonist candidates were predicted using the in silico modeling tool VirtualToxLab. VirtualToxLab utilizes flexible docking combined with multi-dimensional QSAR to predict the binding affinities of compounds to target proteins based on linear regression relationships. These relationships are established between the biotoxicity values of known chemicals (expressed logarithmically) and their molecular structure descriptors, which are used to create the training dataset (Vedani et al., 2015). The VEGA platform, another in silico tool, includes dozens of QSAR models for various toxicological endpoints. In this study, the VEGA QSAR was used to predict androgen receptor (AR), estrogen receptor (ER), glucocorticoid receptor (GR), thyroid hormone receptor (TR) activities, mutagenicity, developmental toxicity, and carcinogenicity for the tentative AhR agonists.

3. Results and discussion

3.1. Organic carbon and total nitrogen contents in sediments

Relatively high OC contents were observed at S9 (11%), followed by S2 (5.4%), S3 (3.3%), and S4 (0.64%) (Fig. S2a). It is worth noting that sites S2, S3, and S4 are influenced by past coal mining activities and research stations and likely exhibit higher OC contents than other sites due to the high OC levels in coal (Cornelissen et al., 2005). TN contents ranged from not detected (N.D.) to 0.16%, with the highest TN contents observed at S2 (0.16%) and S3 (0.10%) (Fig. S2b). Although high OC content was observed in the sediment of S9, TN content was below the detection limit. Site S9 is less influenced by coal and plant debris, but the OC content is high, indicating that further research is needed. The ratio of OC to TN (i.e., C/N ratio) in sediments, excluding those from S6–S9, ranged from 4.4 to 28 (Fig. S2c). Sites S2, S3, and S4, which are affected by coal and other anthropogenic activities, suggest terrestrial organic matter sources, while the other sites indicate marine organic matter sources. Overall, the sediments from Kongsfjorden, particularly those near the coast, appear to exhibit geochemical characteristics reflecting the terrestrial sources.

3.2. AhR-mediated potencies in sediments

The AhR-mediated potencies in REs of sediments from Kongsfjorden showed site-specific variations (Fig. 1b), with notably higher potencies observed at S2 and S3. This increased activity could be attributed to the proximity of these sites to Ny-Ålesund, an area historically associated with coal mining activities, residual coal deposits, and research facilities (Steenhuisen and van den Heuvel-Greve, 2021). It is believed that AhR agonists were mainly derived from these local sources, resulting in relatively high AhR-mediated potencies in the sediments. Silica gel fractionation of S2 and S3 samples revealed that AhR-mediated potencies were higher in F2 and F3 compared to F1 (Fig. 2a), indicating that the major AhR agonists in Kongsfjorden sediments are mid-polar and polar compounds. Similar trends have been observed in sediments from other regions with high levels of industrialization, such as Lake Sihwa, Ulsan Bay, and Yeongil Bay in South Korea, as well as the Yellow Sea and Bohai Sea in China (Cha et al., 2019, 2021; Gwak et al., 2022; Kim et al., 2019; Lee et al., 2022). Previous studies have reported PAH contaminations in Kongsfjorden sediments, primarily from coal mining, residual coal, tourism, and research activities (Jiao et al., 2009; Lee et al., 2023). The significant AhR-mediated potencies observed in the sediments in this study might be attributed to these PAHs; thus, this study focused on identifying mid-polar AhR-active substances (i.e., those containing PAHs) in the sediments of Kongsfjorden.

F2 from S2 and S3 sediment extracts, which exhibited high AhR-mediated potencies, were further fractionated using RP-HPLC (Fig. 2a). The AhR-mediated potencies in the F2 subfractions (F2.1–F2.10) of S2 and S3 were relatively high in fractions F2.6–F2.8, corresponding to compounds with a log K_{OW} of 5–8. These results suggest that the major mid-polar AhR agonists in Kongsfjorden sediments were likely compounds with log K_{OW} between 5 and 8, consistent with previous studies (Cha et al., 2019; Gwak et al., 2022; Kim et al., 2019). Interestingly, AhR-mediated potencies in both the silica gel and RP-HPLC fractions were higher than those in the REs. This may be due to a masking effect, where interfering compounds in the organic extract were removed through fractionation (Hong et al., 2023). The EC_{50} values were calculated from the dose-response curves for F2.6–F2.8 in S2 and S3 (Fig. 2b). The BaP-EQ_{bio} for F2.6–F2.8 from S2 and S3 were 250–2100 ng BaP-EQ g^{-1} dry weight (dw) and 110–4600 ng BaP-EQ g^{-1} dw, respectively. These calculated BaP-EQ_{bio} values were then used for potency balance analysis.

Similar AhR-mediated potencies to those observed in F2 were also

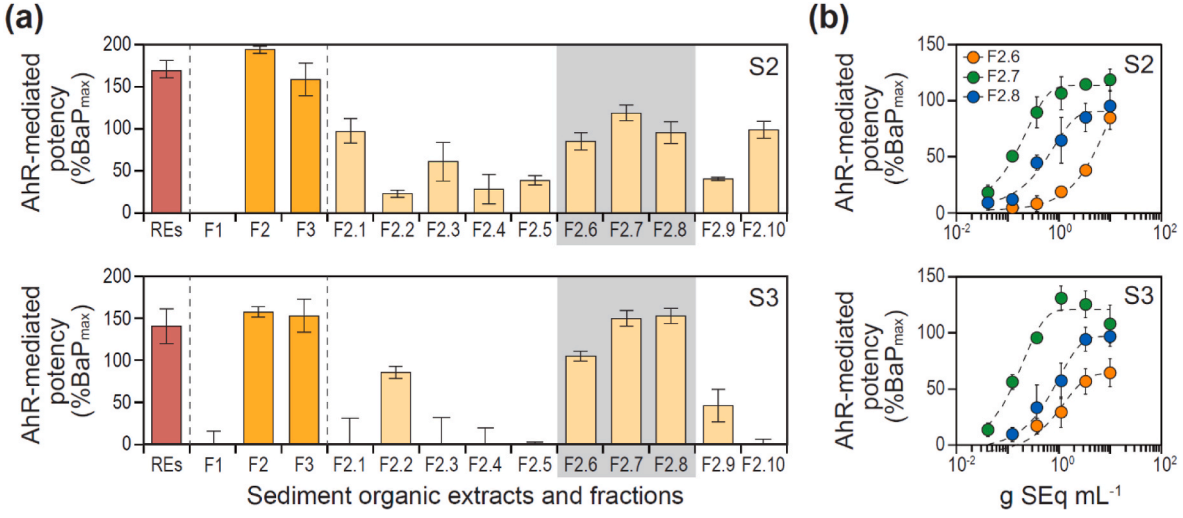

Fig. 2. (a) AhR-mediated potencies in raw organic extracts (REs), silica gel fractions (F1: non-polar, F2: mid-polar, and F3: polar), and RP-HPLC subfractions (F2.1–F2.10) of F2 of sites S2 and S3 sediments collected from Kongsfjorden. **(b)** Dose-response characterization for AhR-mediated potencies of selected RP-HPLC fractions (i.e., F2.6−F2.8) of sites S2 and S3 (Error bar: mean ± standard deviation, n = 3).

found in F3 of the sediment extracts. Previous studies have identified polar AhR agonists in sediments associated with human activities, such as the use of pharmaceuticals and pesticides (Cha et al., 2021). Future research should focus on identifying the major polar AhR-active substances in the sediments of Arctic Svalbard, as well as their sources and biological impacts.

3.3. Distributions of PTSs in sediments

t-PAHs were detected in sediments at all sites in Kongsfjorden, with concentrations ranging from 6.1 to 2100 ng g^{-1} dw (Fig. 3 and Table S7). The highest concentration of t-PAHs was observed at S2 (2100 ng g^{-1} dw), followed by S3 (1900 ng g^{-1} dw). Among the t-PAHs, phenanthrene (Phe) exhibited the highest concentrations at S2 (800 ng g^{-1} dw) and S3 (790 ng g^{-1} dw) (Table S7). Phe has been reported to originate from both natural sources (e.g., wildfires, rocks, and plant roots) and anthropogenic sources (e.g., combustion of fossil fuels) (Boitsov et al., 2009). In this study, high concentrations of Phe were detected in coal residue samples near Ny-Ålesund, indicating that the PAHs in Kongsfjorden sediments, particularly at S2 and S3, are associated with coal residues (Table S8). Previous studies have also reported high concentrations of Phe in coal samples (Howaniec et al., 2018). Concentrations of Phe in the sediments of S2 and S3 exceeded the effect range low (225 ng g^{-1} dw) (MacDonald et al., 2000), suggesting potential ecological effects of Phe in sediments from Kongsfjorden.

The concentrations of e-PAHs in sediments from Kongsfjorden ranged from 0.5 to 1000 ng g^{-1} dw (Fig. 3 and Table S7). Similar to the pattern observed for t-PAHs, S2 (1000 ng g^{-1} dw) and S3 (820 ng g^{-1} dw) showed great concentrations of e-PAHs. In S2, the most prominent e-PAHs were benzo[*b*]naphtho[*2,1-d*]thiophene (BBNT), 11H-benzo[*b*]fluorene (11BbF), and benzo[*b*]naphtho[*2,3-d*]furan (BBNF). In S3 sediment, 11H-benzo[*a*]fluorene (11BaF), BBNF, and 11BbF were predominant (Table S7). 11BaF is known to originate from gasoline engines, BBNT and 11BbF from coal sources (Kim et al., 2019; Koganti et al., 2000; Kumar and Kim, 2000), and BBNF has been reported to originate from oil sources (Jiang et al., 2024). Thus, the e-PAHs in the sediments of S2 and S3 primarily originate from coal, with additional contributions from gasoline engines and oil sources.

The concentrations of alkyl-PAHs in sediments from Kongsfjorden ranged from 47 to 79,000 ng g^{-1} dw (Fig. 3 and Table S7). The highest concentrations were found in the sediments at S2 (79,000 ng g^{-1} dw), followed by S3 (44,000 ng g^{-1} dw) and S4 (6800 ng g^{-1} dw). S2 and S3, sites with coal or abandoned mines, still exhibit high alkyl-PAH levels despite the cessation of mining activities, likely due to the dispersion of mechanical equipment, waste residues, and fine coal particles (Jiao et al., 2009). Among the alkyl-PAHs in S2 and S3, alkyl-Na were the predominant compounds (Table S7). This pattern was also observed in sediments and coal in previous studies (Yunker et al., 2012, 2015). Alkyl-Na are mainly originated from vegetation fires, biological pollutants, crude oil, and coal (Masclet et al., 1986). In the present study, great concentrations of alkyl-Na were also found in the coal samples (Table S8). A previous study reported a similar pattern in soil from the Midtre Lovénbreen glacier foreland in Svalbard (Cha et al., 2024). Overall, similar patterns of alkyl-PAHs contamination were observed in the sediments and coal of Kongsfjorden and in the soils near Ny-Ålesund, Svalbard.

The concentrations of SOs in sediments from Kongsfjorden ranged from 4.2 to 130 ng g^{-1} dw, with the highest concentrations found at S2 (130 ng g^{-1} dw) and S3 (130 ng g^{-1} dw) (Fig. 3 and Table S7). The high concentrations of SOs at S2 and S3 are likely due to the input of plastics from nearby residential areas and research stations. In addition, SOs are known to be compounds capable of traveling long distances through ocean currents, raising the possibility that SOs used indiscriminately in neighboring European countries may have been transported over long distances (Kwon et al., 2015). To date, research on the distribution of SOs in environmental media within the Arctic region and Europe remains limited. Thus, further investigations are needed to accurately identify the sources and causes of SOs pollution.

Overall, PTS concentrations in the sediments of Kongsfjorden were relatively high at S2 and S3. Typically, OC content and PTS concentrations in sediments are positively correlated, and this study confirmed a significant positive correlation at all sites except S9, where OC content was abnormally high. The S2, S3, and S4 showed more severe contamination by AhR-active substances compared to other regions, likely due to local sources such as coal residues rather than long-distance transport. With accelerating climate change, permafrost thaw or glacial retreat may lead to glacial/fluvial runoff sweeping through coal deposit regions and infiltrating the Kongsfjorden environment (Ademollo et al., 2021; Cha et al., 2024). This could further accelerate the influx of coal-derived AhR agonists into the marine environment. Thus, ongoing monitoring of AhR-active substances in Kongsfjorden environments is necessary.

3.4. Potential sources of PAHs in sediments

PCA-MLR analysis identified coal (Factor 1), petroleum combustion (Factor 2), and coal combustion (Factor 3) as the primary sources of PAHs in Kongsfjorden sediments (Fig. 4a and Table S9). Factor 1, dominated by Phe, was closely associated with coal (Lee et al., 2023). Factor 2, dominated by pyrene, indicated petroleum combustion (Harrison et al., 1996), while Factor 3, dominated by benzo[*b*]

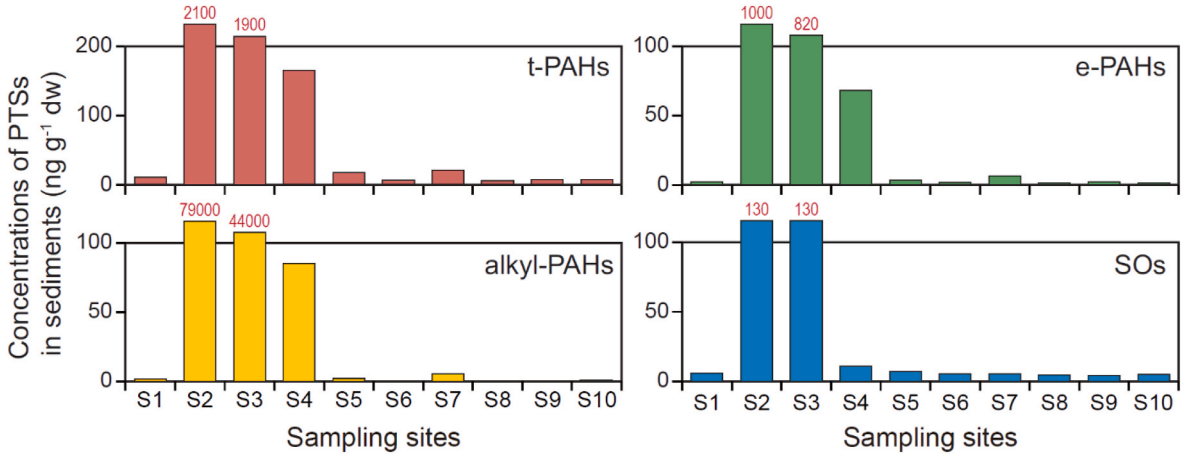

Fig. 3. Concentrations of persistent toxic substances (PTSs), such as 15 traditional PAHs (t-PAHs), 14 emerging PAHs (e-PAHs), 20 alkyl-PAHs, and 10 styrene oligomers (SOs), in sediments from Kongsfjorden.

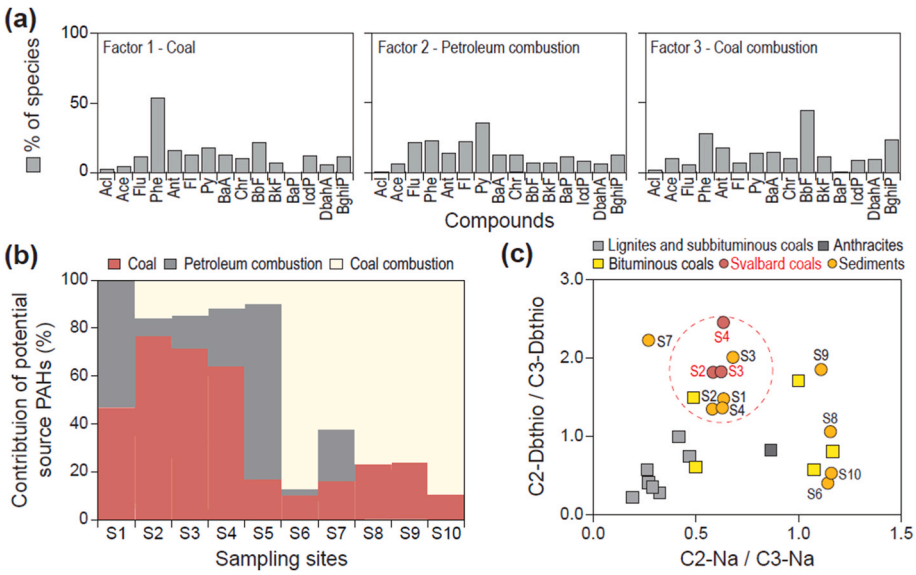

Fig. 4. (a) Potential sources of PAHs in sediments from Kongsfjorden derived using principal component analysis (PCA) with multiple linear regression (MLR) (Factor 1: coal, Factor 2: petroleum combustion, and Factor 3: coal combustion) (details are provided in Table S9). **(b)** The contribution of potential sources (i.e., coal, petroleum combustion, and coal combustion) of PAHs in the sediments from Kongsfjorden **(c)** Diagnostic double ratios of alkyl-PAHs (i.e., C2–Na/C3–Na and C2-Dbthio/C3-Dbthio). in sediments and coals from Kongsfjorden and those in various coal samples reported previously (Hindersmann and Achten, 2018; Pies et al., 2008; Yunker et al., 2002).

fluoranthene, suggested coal combustion (Kwon and Choi, 2014). These sources were associated with abandoned mines and coal residues near Ny-Ålesund and local anthropogenic activities. The contributions of Factor 1, Factor 2, and Factor 3 were 39% from coal, 39% from petroleum combustion, and 20% from coal combustion, respectively. The source apportionment revealed that PAHs in sediments at S2 and S3 were predominantly from residual coal (Fig. 4b). The petroleum combustion source was identified in sediments from S1–S7, likely due to the influx from ships related to tourism and cargo transport (Paglia, 2020). In contrast, sediments from S8–S10 were primarily influenced by coal combustion.

To distinguish between petrogenic and pyrogenic sources, the isomer patterns of alkyl-PAHs were analyzed (Yunker et al., 2012, 2015) (Fig. S3). Na, dibenzothiophene (Dbthio), and chrysene (Chr) exhibited a bell-shaped distribution pattern, indicative of petrogenic origin (Hong et al., 2012). Petrogenic PAHs, typically originating from coal and oil under low-temperature conditions, were identified (Yunker et al., 2015). In contrast, fluoranthene and Phe exhibited patterns where alkylation decreased with increasing substitution, characteristic of pyrogenic PAHs, primarily derived from coal tar (Yunker et al., 2015). The distribution patterns of alkyl-PAHs in the sediments were consistent with those found in coal (Table S8 and Fig. S3). Further analysis using the C2-Dbthio/C3-Dbthio and C2–Na/C3–Na ratios confirmed that the alkyl-PAHs composition in sediments from S1–S4 was predominantly similar to bituminous coal (Fig. 4c). Bituminous coal has been reported to contain PAHs ranging from hundreds to thousands of mg kg^{-1} (Lee et al., 2023), suggesting it as a potential source of AhR agonists in sediment samples (Meyer et al., 2014).

3.5. Potency balance analysis

The concentrations of target AhR agonists in the F2.6–F2.8 of S2 and S3 ranged from 7.3 to 1000 ng g^{-1} dw and 5.6–820 ng g^{-1} dw, respectively (Table S10). In these subfractions, BBNF was the predominant AhR agonist in F2.6, while BBNT and 11BbF dominated in F2.7 for S2 and S3, respectively. The BaP-EQ_{chem} concentrations in F2.6–F2.8 were 22–1100 ng g^{-1} dw for S2 and 17–970 ng g^{-1} dw for S3. Benzo[*b*] anthracene (BbA) contributed the highest BaP-EQ_{chem} concentration in F2.6 of both sites, whereas 1-methylchrysene (1MC) was dominant in F2.7. Despite lower concentrations, BbA and 1MC significantly contributed to the BaP-EQ_{chem} concentrations due to their higher AhR binding affinities relative to BaP. Potency balance analysis indicated that the target AhR agonists in F2.6 of S2 and S3 accounted for over 100% of the observed AhR-mediated potency (Fig. 5a and Table S11), with BbA being the primary contributor. When BaP-EQ_{chem} is significantly greater than BaP-EQ_{bio}, mixture toxic effects are suspected (Hong et al., 2023). Previous studies have also shown a tendency for BaP-EQ_{chem} to exceed BaP-EQ_{bio} (Gwak et al., 2022, 2024; Hashmi et al., 2018). Since potency balance analysis assumes that the effects of toxic substances are additive, it may not fully explain the mixture effects of compounds. Thus, future studies should evaluate mixture effects by measuring AhR-mediated potencies in recombined samples. In F2.7, the target AhR agonists explained 52% and 21% of the AhR-mediated potencies in S2 and S3, respectively, primarily from 1MC (27%) and 3-methylchrysene (8.3%) in S2, and from 1MC (18%) and 4,5-methanochrysene (8.6%) in S3. Additionally, 20-methylcholanthrene contributed 4.5% and 3.2% of the AhR-mediated potencies in F2.8 of S2 and S3, respectively. These findings suggest that while known AhR agonists in F2.6 fully account for the observed AhR-mediated potencies, those in F2.7 and F2.8 do not, implying the presence of unmonitored AhR agonists in the sediments of Kongsfjorden.

3.6. Nontarget screening of highly potent fractions

NTS using GC-QTOFMS was performed to identify tentative AhR agonists in the subfractions of F2 (F2.4–F2.8 of S2), including highly potent fractions (Fig. 5b). The selection of these tentative AhR agonists followed a four-step criterion. First, 1327 to 2993 peaks were detected across F2.4–F2.8 fractions of S2. In the second step, 189 to 519 compounds were matched with library software. In the third step, compounds with a matching score of ≥80 were selected, resulting in the detection of 73–287 compounds across the fractions. Finally, compounds with three or more aromatic rings were chosen, as AhR agonists typically possess aromatic rings (Cheng et al., 2024). This process led to the selection of 1, 6, 22, 14, and 5 compounds in F2.4–F2.8, respectively. Among the 48 tentative AhR agonists selected, their origins were traced to coal (n = 27), oil (n = 5), rock (n = 1), natural product (n = 2), and plastic (n = 1) (details in Table 1 and Fig. 5c). Twelve compounds

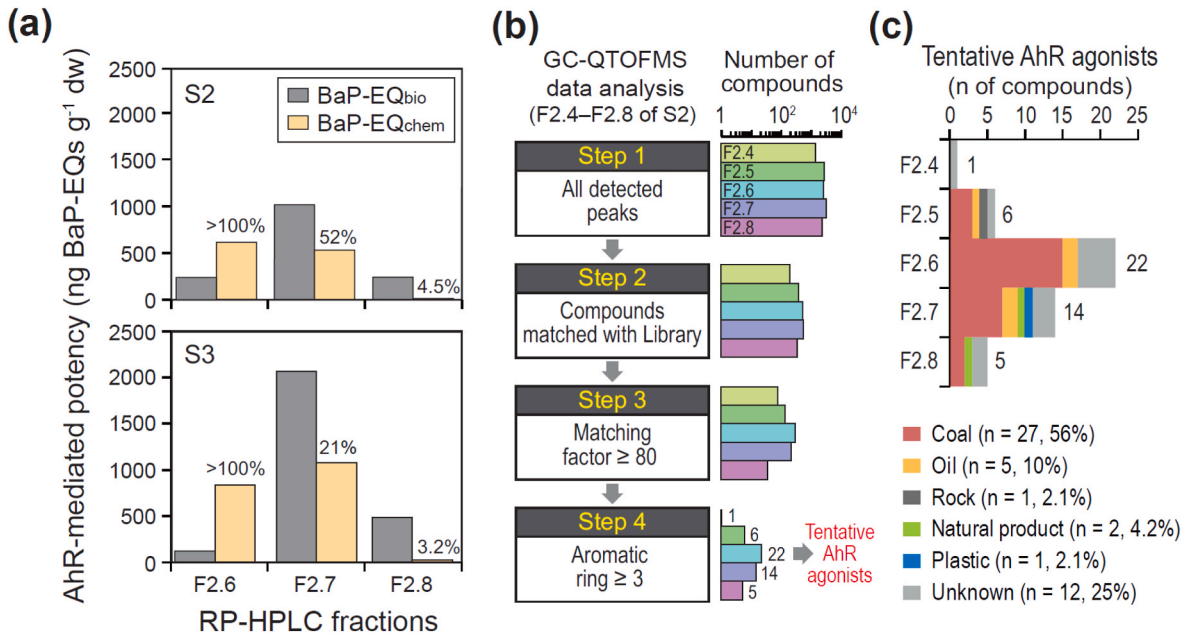

Fig. 5. (a) Contributions of target AhR agonists (instrument-derived BaP-EQs, BaP-EQ_{chem}) to the total induced AhR-mediated potencies (bioassay-derived BaP-EQs, BaP-EQ_{bio}) in F2.6–F2.8 of sites S2 and S3 (details are provided in Table S11). **(b)** Procedures of nontarget screening data analysis (F2.4–F2.8 of S2) for the selection of AhR agonist candidates. **(c)** Origin of 48 tentative AhR agonists (The full list of compounds is shown in Table 1).

remained unidentified. The predominance of coal-derived compounds among the tentative AhR agonists suggests that these agonists likely originated from surrounding coal deposits and abandoned mines, contributing to the AhR-mediated potencies observed in the sediments.

3.7. Prediction of potential toxicities of AhR agonist candidates using QSAR modeling

The AhR binding affinities of 48 AhR agonist candidates were predicted using VirtualToxLab (Table 1). Among these, one compound exhibited high AhR binding affinity, 16 compounds showed moderate affinity, and 26 compounds exhibited low affinity. The compound with the highest AhR binding affinity, 2-(4-phenoxyphenoxy)ethyl benzoate, originated from oil and was likely introduced by a nearby ship (Alvarez et al., 2017). Of the 16 compounds with moderate AhR binding affinity, seven were identified as coal-derived, predominantly from bituminous coal (Li et al., 2019; Meyer et al., 2014). Previous studies have confirmed that bituminous coal can induce mutagenicity and carcinogenicity, along with AhR-mediated effects (Li et al., 2019; Meyer et al., 2014). The toxicity potential of the 43 tentative AhR agonists (0.292–0.571) was comparable to that of the target AhR agonists (0.367–0.474) (Table S12), suggesting that these compounds are likely contributors to AhR-mediated potencies in sediments.

Additional toxicities for the 48 tentative AhR agonists were predicted using the VEGA QSAR model (Table S13). All 48 compounds were identified as carcinogenic, though GR and TR activities were not predicted. Some compounds were predicted to exhibit AR activity, ER activity, mutagenicity, and carcinogenicity. However, it is important to note the limitations of these models. VirtualToxLab assesses binding affinity based on receptor conditions, which may not fully replicate those in living organisms (Vedani et al., 2015). The VEGA QSAR model, which relies on existing database information, also has limitations in predicting the toxicity of novel compounds (Jagiello et al., 2016). Future research should focus on the toxicological validation of these tentative AhR agonists.

4. Conclusion

This study identified major AhR agonists in Kongsfjorden sediments using EDA, demonstrating the effective application of effect-based monitoring (EBM). Additionally, NTS identified potential AhR agonists derived from coal. The Kongsfjorden environment exhibits distinctive geochemical characteristics, with varying concentrations and distinct sources of PTSs across different sites. Sediment pollution in this region is primarily attributed to coal remnants on land. As climate change accelerates, glacio-fluvial runoff may increasingly transport these coal residues into Kongsfjorden, posing significant ecological risks to marine organisms due to the AhR-binding potential of coal-derived substances. Therefore, further research on the influx, behavior, and ecological impacts of coal-derived substances is essential. Quantitative measurement of coal-derived substances, facilitated by EBM, can enhance our understanding of the potential ecological risks to the Kongsfjorden ecosystem and support the development of effective environmental response strategies.

CRediT authorship contribution statement

Jiyun Gwak: Writing – original draft, Visualization, Investigation, Formal analysis, Data curation, Conceptualization. **Jihyun Cha:** Writing – original draft, Visualization, Investigation, Formal analysis, Data curation, Conceptualization. **Seung-Il Nam:** Writing – review & editing, Project administration, Funding acquisition. **Jung-Hyun Kim:** Writing – review & editing, Investigation, Formal analysis, Data curation. **Junghyun Lee:** Writing – review & editing, Formal analysis, Data curation. **Hyo-Bang Moon:** Writing – review & editing, Formal analysis, Data curation. **Jong Seong Khim:** Writing – review & editing, Project administration, Funding acquisition. **Seongjin Hong:** Writing – review & editing, Visualization, Supervision, Project administration, Investigation, Funding acquisition, Formal analysis, Data curation, Conceptualization.

Declaration of competing interest

The authors declare that they have no known competing financial

Table 1
List of 48 tentative AhR agonists in F2.4–F2.8 of S2 sediment using GC-QTOFMS, and their origin and toxic potentials predicted using VirtualToxLab modeling.

Compounds	Molecular formula	Molecular weight	Origin	References	Toxic potential[a]
F2.4					
8-Methyl-2H-pyrano[*2,3-b*]quinoline	$C_{13}H_{11}NO$	197.23	-[b]	-	-
F2.5					
9-Ethyl-9,10-dihydroanthracene	$C_{16}H_{16}$	208.29	Coal	Li et al. (2017)	0.371
1-Methylphenanthrene	$C_{15}H_{12}$	192.26	Coal	Kvalheim et al. (1987)	0.315
3-Methylphenanthrene	$C_{15}H_{12}$	192.26	Coal	Kvalheim et al. (1987)	0.313
9,10-Dihydroanthracene	$C_{14}H_{12}$	180.24	Oil	Alvarez et al. (2017)	0.308
Phenylnaphthalene	$C_{16}H_{12}$	204.27	Rock	Marynowski et al. (2001)	0.405
9,9-Dimethyl-9H-xanthen	$C_{15}H_{14}O$	210.27	-	-	-
F2.6					
1,7-Dimethylphenanthrene	$C_{16}H_{14}$	206.28	Coal	Sun et al. (2013)	0.328
1-Methylphenanthro[*4,5-bcd*]thiophene	$C_{15}H_{10}S$	222.31	Coal	Zhao et al. (2021)	0.292
1-Methylpyrene	$C_{17}H_{12}$	216.28	Coal	Li et al. (2011)	0.313
2,3,5-Trimethylphenanthrene	$C_{17}H_{16}$	220.31	Coal	Jerković et al. (2011)	0.321
2,3-Dimethylphenanthrene	$C_{16}H_{14}$	206.28	Coal	Sun et al. (2013)	0.340
2,5-Dimethylphenanthrene	$C_{16}H_{14}$	206.28	Coal	Qiu et al. (2019)	0.310
2,7-Dimethylanthracene	$C_{16}H_{14}$	206.28	Coal	Ostojić et al. (2014)	0.338
2-Benzylnaphthalin	$C_{17}H_{14}$	218.29	Coal	Taylor and Bell (1980)	-
2-Phenyldibenzofuran	$C_{18}H_{12}O$	244.29	Coal	Yang et al. (2017)	0.489
3,6-Dimethylphenanthrene	$C_{16}H_{14}$	206.28	Coal	Fan et al. (2017)	0.317
4-Methylpyrene	$C_{17}H_{12}$	216.28	Coal	Li et al. (2011)	0.311
4-Phenyldibenzofuran	$C_{18}H_{12}O$	244.29	Coal	Meyer zu Reckendorf (2000)	0.484
9-Ethylanthracene	$C_{16}H_{14}$	206.28	Coal	Kidena et al. (2000)	0.359
9-sec-Butyl-9,10-dihydroanthracen	$C_{18}H_{20}$	236.35	Coal	Fan et al. (2017)	0.386
9-Vinylanthracene	$C_{16}H_{12}$	204.27	Coal	Li et al. (2020)	0.361
1,2,3,4,5,6-Hexahydroanthracene	$C_{14}H_{16}$	184.28	Oil	Alvarez et al. (2017)	0.340
2-(4-Phenoxyphenoxy)ethyl benzoate	$C_{21}H_{18}$	334.37	Oil	Alvarez et al. (2017)	0.571
2-(2-Methylphenyl)naphthalene	$C_{17}H_{14}$	218.29	-	-	0.412
4,5-Dimethylphenanthrene	$C_{16}H_{14}$	206.28	-	-	0.317
5,12-Dihydrotetracene	$C_{18}H_{14}$	230.30	-	-	0.421
6,13-Dihydrodibenzo[*b,i*]phenazine	$C_{20}H_{14}N_2$	282.34	-	-	0.417
9,10-Dimethylphenanthren	$C_{16}H_{14}$	206.28	-	-	0.345
F2.7					
1,12-Dimethylbenzo[*c*]phenanthrene	$C_{20}H_{16}$	256.34	Coal	Wu et al. (2023)	0.362
1-Methylbenzo[*c*]phenanthrene	$C_{19}H_{14}$	242.31	Coal	Chen et al (2017)	0.388
2,3,6,7-Tetramethylanthracene	$C_{18}H_{18}$	234.34	Coal	Ellison and Hey (1938)	0.343
2,4,5,7-Tetramethylphenanthrene	$C_{18}H_{18}$	234.34	Coal	Bongers et al. (1998)	0.345
2-Isopropyl-10-methylphenanthrene	$C_{18}H_{18}$	234.34	Coal	He et al. (2023)	0.414
2-Methyltriphenylene	$C_{19}H_{14}$	242.31	Coal	Russo et al. (2019)	0.372
Benzo[*e*]pyrene	$C_{20}H_{12}$	252.31	Coal	Fan et al. (2017)	0.376
Gossypol	$C_{30}H_{30}O_8$	518.55	Natural product	Keshmiri-Neghab and Goliaei (2014)	0.117
8-Isopropyl-1,3-dimethylphenanthrene	$C_{19}H_{20}$	248.36	Oil	Zhang et al. (2017)	0.392
Retene	$C_{18}H_{18}$	234.34	Oil	Zhang et al. (2017)	0.419
Tri-m-tolyl phosphate	$C_{21}H_{21}O_4P$	368.36	Plastic	Ngai and Plazek (2002)	0.168
1,2'-Binaphthalene	$C_{20}H_{14}$	254.33	-	-	0.482
10,18-Bisnorabieta-8,11,13-triene	$C_{18}H_{26}$	242.40	-	-	0.439
12-Ethyltetraphene	$C_{20}H_{16}$	256.34	-	-	0.411
F2.8					
Anthanthrene	$C_{22}H_{12}$	276.33	Coal	Platt et al. (2002)	0.404
Simonellite	$C_{19}H_{24}$	252.39	Coal	Lu et al. (2019)	0.416
Nordehydroabietane	$C_{19}H_{28}$	256.40	Natural product	Öztürk et al. (2009)	0.425
3,3,7-trimethyl-2,4-dihydro-1H-chrysene	$C_{21}H_{22}$	274.40	-	-	0.411
10,18-Bisnorabieta-5,7,9(10),11,13-pentaene	$C_{18}H_{22}$	238.37	-	-	0.413

[a] 0.0−0.2: none binding, 0.2−0.4: low binding, 0.2−0.4: moderate binding, 0.4−0.6: elevated binding.
[b] n.a: not available.

interests or personal relationships that could have appeared to influence the work reported in this paper.

Acknowledgments

This study was supported by grants from the National Research Foundation of Korea (NRF-2021M1A5A1075514; KOPRI-PN24013) and the Ministry of Oceans and Fisheries (RS-2024-00417889 and RS-2021-KS211469). This work was also supported by the research fund of Chungnam National University.

Appendix A. Supplementary data

Supplementary data to this article can be found online at https://doi.org/10.1016/j.chemosphere.2024.143771.

Data availability

Data will be made available on request.

References

Alvarez, J.O., Saputra, I.W.R., hechter, D.S., 2017. Potential of improving oil recovery with surfactant additives to completion fluids for the Bakken. Energy Fuels 31 (6), 5982–5994. https://doi.org/10.1021/acs.energyfuels.7b00573.

Ademollo, N., Spataro, F., Rauseo, J., Pescatore, T., Fattorini, N., Valsecchi, S., Polesello, S., Patrolecco, L., 2021. Occurrence, distribution and pollution pattern of legacy and emerging organic pollutants in surface water of the Kongsfjorden (Svalbard, Norway): environmental contamination, seasonal trend and climate change. Mar. Pollut. Bull. 163, 111900. https://doi.org/10.1016/j.marpolbul.2020.111900.

Bletsou, A.A., Jeon, J., Hollender, J., Archontaki, E., Thomaidis, N.S., 2015. Targeted and non-targeted liquid chromatography-mass spectrometric workflows for identification of transformation products of emerging pollutants in the aquatic

environment. Trends Anal. Chem. 66, 32–44. https://doi.org/10.1016/j.trac.2014.11.009.
Boitsov, S., Jensen, H.K.B., Klungsøyr, J., 2009. Natural background and anthropogenic inputs of polycyclic aromatic hydrocarbons (PAH) in sediments of South-Western Barents Sea. Mar. Environ. Res. 68 (5), 236–245. https://doi.org/10.1016/j.marenvres.2009.06.013.
Bongers, G.D., Jackson, W.R., Woskoboenko, F., 1998. Pressurised steam drying of Australian low-rank coals: Part 1. Equilibrium moisture contents. Fuel Process. Technol. 57 (1), 41–54. https://doi.org/10.1016/S0378-3820(98)00066-6.
Ccanccapa-Cartagena, A., Pico, Y., Ortiz, X., Reiner, E.J., 2019. Suspect, non-target and target screening of emerging pollutants using data independent acquisition: assessment of a Mediterranean River basin. Sci. Total Environ. 687, 355–368. https://doi.org/10.1016/j.scitotenv.2019.06.057.
Cha, J., Hong, S., Kim, J., Lee, J., Yoon, S.J., Lee, S., Moon, H.-B., Shin, K.-H., Hur, J., Giesy, J.P., Khim, J.S., 2019. Major AhR-active chemicals in sediments of Lake Sihwa, South Korea: application of effect-directed analysis combined with full-scan screening analysis. Environ. Int. 133, 105199. https://doi.org/10.1016/j.envint.2019.105199.
Cha, J., Hong, S., Lee, J., Gwak, J., Kim, M., Kim, T., Hur, J., Giesy, J.P., Khim, J.S., 2021. Novel polar AhR-active chemicals detected in sediments of an industrial area using effect-directed analysis based on in vitro bioassays with full-scan high resolution mass spectrometric screening. Sci. Total Environ. 779, 146566. https://doi.org/10.1016/j.scitotenv.2021.146566.
Cha, J., Kim, J.-H., Jung, J.Y., Nam, S.-I., Hong, S., 2024. Chronological distribution and potential sources of persistent toxic substances in soils from the glacier foreland of Midtre Lovénbreen, Svalbard. Environ. Pollut. 357, 124387. https://doi.org/10.1016/j.envpol.2024.124387.
Chen, W., Wu, X., Zhang, H., Sun, J., Liu, W., Zhu, L., Li, X., Tsang, D.C.W., Tao, S., Wang, X., 2017. Contamination characteristics and source apportionment of methylated PAHs in agricultural soils from Yangtze River Delta, China. Environ. Pollut. 230, 927–935. https://doi.org/10.1016/j.envpol.2017.07.035.
Cheng, F., Escher, B.I., Li, H., König, M., Tong, Y., Huang, J., He, L., Wu, X., Lou, X., Wang, D., Wu, F., Pei, Y., Yu, Z., Brooks, B.W., Zeng, E.Y., You, J., 2024. Deep learning bridged bioactivity, structure, and GC-HRMS-readable evidence to decipher nontarget toxicants in sediments. Environ. Sci. Technol. https://doi.org/10.1021/acs.est.3c10814.
Choi, Y., Seo, C.-D., Lee, W., Son, H., Lee, Y., 2024. Assessment of bioactive chemicals in wastewater effluents and surface waters using in vitro bioassays in the Nakdong River basin, Korea. Chemosphere 347, 140621. https://doi.org/10.1016/j.chemosphere.2023.140621.
Cornelissen, G., Gustafsson, Ö., Bucheli, T.D., Jonker, M.T.O., Koelmans, A.A., van Noort, P.C.M., 2005. Extensive sorption of organic compounds to black carbon, coal, and kerogen in sediments and soils: mechanisms and consequences for distribution, bioaccumulation, and biodegradation. Environ. Sci. Technol. 39 (18), 6881–6895. https://doi.org/10.1021/es050191b.
Dowdall, M., Vicat, K., Frearson, I., Gerland, S., Lind, B., Shaw, G., 2004. Assessment of the radiological impacts of historical coal mining operations on the environment of Ny-Ålesund, Svalbard. J. Environ. Radioact. 71 (2), 101–114. https://doi.org/10.1016/S0265-931X(03)00144-9.
Eichbaum, K., Brinkmann, M., Buchinger, S., Reifferscheid, G., Hecker, M., Giesy, J.P., Engwall, M., van Bavel, B., Hollert, H., 2014. In vitro bioassays for detecting dioxin-like activity — application potentials and limits of detection, a review. Sci. Total Environ. 487. https://doi.org/10.1016/j.scitotenv.2014.03.057, 371–48.
Ellison, H., Hey, D.H., 1938. 345. The action of benzaldehyde on o-, m-, and p-xylene in the presence of aluminium chloride. J. Chem. Soc. Chem. (0), 1847–1853. https://doi.org/10.1016/j.scitotenv.2014.03.057.
Fan, X., Fei, Y., Chen, L., Li, W., 2017. Distribution and structural analysis of polycyclic aromatic hydrocarbons abundant in coal tar pitch. Energy Fuels 31 (5), 4694–4704. https://doi.org/10.1021/acs.energyfuels.6b03113.
Feng, J., Li, X., Guo, W., Liu, S., Ren, X., Sun, J., 2014. Potential source apportionment of polycyclic aromatic hydrocarbons in surface sediments from the middle and lower reaches of the Yellow River, China. Environ. Sci. Pollut. Res. 21, 11447–11456. https://doi.org/10.1007/s11356-014-3051-0.
Ghosh, P., Gupta, A., Thakur, I.S., 2015. Combined chemical and toxicological evaluation of leachate from municipal solid waste landfill sites of Delhi, India. Environ. Sci. Pollut. Res. 22 (12), 9148–9158. https://doi.org/10.1007/s11356-015-4077-7.
Gwak, J., Cha, J., Lee, J., Kim, Y., An, S.-A., Lee, S., Moon, H.-B., Hur, J., Giesy, J.P., Hong, S., Khim, J.S., 2022. Effect-directed identification of novel aryl hydrocarbon receptor-active aromatic compounds in coastal sediments collected from a highly industrialized area. Sci. Total Environ. 803, 149969. https://doi.org/10.1016/j.scitotenv.2021.149969.
Gwak, J., Lee, J., Cha, J., Moon, H.B., Khim, J.S., Hong, S., 2024. Effect-directed analysis and nontarget screening for identifying AhR-active substances in sediments of Gamcheon Harbor, South Korea. Mar. Pollut. Bull. 209, 117081. https://doi.org/10.1016/j.marpolbul.2024.117081.
Han, B., Gao, W., Li, Q., Liu, A., Gong, J., Zheng, Y., Wang, N., Zheng, L., 2022. Residues of persistent toxic substances in surface soils of Ny-Ålesund in the arctic: occurrence, source, and ecological risk assessment. Chemosphere 303, 135092. https://doi.org/10.1016/j.chemosphere.2022.135092.
Harrison, R.M., Smith, D.J.T., Luhana, L., 1996. Source apportionment of atmospheric polycyclic aromatic hydrocarbons collected from an urban location in birmingham, U.K. Environ. Sci. Technol. 30 (3), 825–832. https://doi.org/10.1021/es950252d.
Hashmi, M.A.K., Escher, B.I., Krauss, M., Teodorovic, I., Brack, W., 2018. Effect-directed analysis (EDA) of Danube River water sample receiving untreated municipal wastewater from Novi Sad, Serbia. Sci. Total Environ. 624, 1072–1081. https://doi.org/10.1016/j.scitotenv.2017.12.187.
Hong, S., Khim, J.S., Ryu, J., Park, J., Song, S.J., Kwon, B.-O., Choi, K., Ji, K., Seo, J., Lee, S., Park, J., Lee, W., Choi, Y., Lee, K.T., Kim, C.-K., Shim, W.J., Naile, J.E., Giesy, J.P., 2012. Two years after the hebei spirit oil spill: residual crude-derived hydrocarbons and potential AhR-mediated activities in coastal sediments. Environ. Sci. Technol. 46 (3), 1406–1414. https://doi.org/10.1021/es203491b.
Hong, S., Lee, J., Lee, C., Yoon, S.J., Jeon, S., Kwon, B.-O., Lee, J.-H., Giesy, J.P., Khim, J.S., 2016. Are styrene oligomers in coastal sediments of an industrial area aryl hydrocarbon-receptor agonists? Environ. Pollut. 213, 913–921. https://doi.org/10.1016/j.envpol.2016.03.025.
Hong, S., Lee, J., Cha, J., Gwak, J., Khim, J.S., 2023. Effect-directed analysis combined with nontarget screening to identify unmonitored toxic substances in the environment. Environ. Sci. Technol. 57 (48), 19148–19155. https://doi.org/10.1021/acs.est.3c05035.
Hopke, P.K., 2003. Recent developments in receptor modeling. J. Chemom. 17 (5), 255–265. https://doi.org/10.1002/cem.796.
Howaniec, N., Kuna-Gwoździewicz, P., Smoliński, A., 2018. Assessment of emission of selected gaseous components from coal processing waste storage site. Sustainability 10. https://doi.org/10.3390/su10030744.
Jagiello, K., Grzonkowska, M., Swirog, M., Ahmed, L., Rasulev, B., Avramopoulos, A., Papadopoulos, M.G., Leszczynski, J., Puzyn, T., 2016. Advantages and limitations of classic and 3D QSAR approaches in nano-QSAR studies based on biological activity of fullerene derivatives. J. Nanoparticle Res. 18 (9), 256. https://doi.org/10.1007/s11051-016-3564-1.
Jiang, L., Nytoft, H.P., Kampoli, I., George, S.C., 2024. Distribution, occurrence and identification of dibenzofuran, benzo[b]naphthofurans and their alkyl derivatives in Gippsland Basin source rocks. Org. Geochem. 187, 104708. https://doi.org/10.1016/j.orggeochem.2023.104708.
Jiao, L., Zheng, G.J., Minh, T.B., Richardson, B., Chen, L., Zhang, Y., Yeung, L.W., Lam, J.C.W., Yang, X., Lam, P.K.S., Wong, M.H., 2009. Persistent toxic substances in remote lake and coastal sediments from Svalbard, Norwegian Arctic: levels, sources and fluxes. Environ. Pollut. 157 (4), 1342–1351. https://doi.org/10.1016/j.envpol.2008.11.030.
Jerković, I., Marijanović, Z., Gugić, M., Roje, M., 2011. Chemical profile of the organic residue from ancient amphora found in the Adriatic Sea determined by direct GC and GC-MS analysis. Molecules 16 (9), 7936–7948. https://doi.org/10.3390/molecules16097936.
Keshmiri-Neghab, H., Goliaei, B., 2014. Therapeutic potential of gossypol: an overview. Pharm. Biol. 52 (1), 124–128. https://doi.org/10.3109/13880209.2013.832776.
Kim, J., Hong, S., Cha, J., Lee, J., Kim, T., Lee, S., Moon, H.-B., Shin, K.-H., Hur, J., Lee, J.-S., Giesy, J.P., Khim, J.S., 2019. Newly identified AhR-active compounds in the sediments of an industrial area using effect-directed analysis. Environ. Sci. Technol. 53 (17), 10043–10052. https://doi.org/10.1021/acs.est.9b02166.
Koganti, A., Singh, R., Rozett, K., Modi, N., Goldstein, L.S., Roy, T.A., Zhang, F.J., Harvey, R.G., Weyand, E.H., 2000. 7H-benzo[c]fluorene: a major DNA adduct-forming component of coal tar. Carcinogenesis 21 (8), 1601–1609. https://doi.org/10.1093/carcin/21.8.1601.
Kumar, S., Kim, T.-Y., 2000. An improved and regiospecific synthesis of trans-3,4-dihydrodiol metabolite of benzo[b]naphtho[2,1-d]thiophene. J. Org. Chem. 65 (12), 3883–3884. https://doi.org/10.1021/jo991933k.
Kvalheim, O.M., Christy, A.A., Telnæs, N., Bjørseth, A., 1987. Maturity determination of organic matter in coals using the methylphenanthrene distribution. Geochem. Cosmochim. Acta 51 (7), 1883–1888. https://doi.org/10.1016/0016-7037(87)90179-7.
Kwon, B.G., Koizumi, K., Chung, S.-Y., Kodera, Y., Kim, J.-O., Saido, K., 2015. Global styrene oligomers monitoring as new chemical contamination from polystyrene plastic marine pollution. J. Hazard Mater. 300, 359–367. https://doi.org/10.1016/j.jhazmat.2015.07.039.
Kwon, H.-O., Choi, S.-D., 2014. Polycyclic aromatic hydrocarbons (PAHs) in soils from a multi-industrial city, South Korea. Sci. Total Environ. 1494–1501. https://doi.org/10.1016/j.jhazmat.2015.07.039.
Kidena, K., Bandoh, N., Kouchi, M., Murata, S., Nomura, M., 2000. Methyl group migration during heat treatment of coal in the presence of polycyclic aromatic compounds. Fuel 79 (3–4), 317–322. https://doi.org/10.1016/S0016-2361(99)00166-0.
Lee, J., Hong, S., Kim, T., Park, S.Y., Cha, J., Kim, Y., Gwak, J., Lee, S., Moon, H.-B., Hu, W., Wang, T., Giesy, J.P., Khim, J.S., 2022. Identification of AhR agonists in sediments of the Bohai and Yellow Seas using advanced effect-directed analysis and in silico prediction. J. Hazard Mater. 435, 128908. https://doi.org/10.1016/j.jhazmat.2022.128908.
Lee, J., Kim, Y., Cha, J., Kim, D., Jang, K., Kim, J.-H., Nam, S.-I., Hong, S., 2023. Distributions and potential sources of polychlorinated biphenyls and polycyclic aromatic hydrocarbons in the glacimarine sediments of Arctic Svalbard. Mar. Pollut. Bull. 189, 114740. https://doi.org/10.1016/j.marpolbul.2023.114740.
Li, Z., Wu, Y., Zhao, Y., Wang, L., Zhu, H., Qin, L., Feng, F., Wang, W., Wu, Y., 2011. Analysis of coal tar pitch and smoke extract components and their cytotoxicity on human bronchial epithelial cells. J. Hazard Mater. 186 (2), 1277–1282. https://doi.org/10.1016/j.jhazmat.2010.11.123.
Li, S., Zong, Z.-M., Li, Z.-K., Wang, S.-K., Yang, Z., Xu, M.-L., Shi, C., Wei, X.-Y., Wang, Y.-G., 2017. Sequential thermal dissolution and alkanolyses of extraction residue from Xinghe lignite. Fuel Process. Technol. 167, 425–430. https://doi.org/10.1016/j.fuproc.2017.07.025.
Li, J., Ran, J., Chen, L.-C., Costa, M., Huang, Y., Chen, X., Tian, L., 2019. Bituminous coal combustion and Xuan Wei Lung cancer: a review of the epidemiology, intervention, carcinogens, and carcinogenesis. Arch. Toxicol. 93 (3), 573–583. https://doi.org/10.1007/s00204-019-02392-y.

Li, W., Wu, J., Huang, X., 2020. Facile fabrication of functional groups-rich sorbent for the efficient enrichment of aromatic N- and S-containing compounds in environmental waters. Anal. Chim. Acta 1113, 36–42. https://doi.org/10.1016/j.aca.2020.03.056.

Lin, Y., Cen, Z., Peng, J., Yu, H., Huang, P., Huang, Q., Lu, Z., Liu, M., Ke, H., Cai, M., 2022. Occurrence and sources of microplastics and polycyclic aromatic hydrocarbons in surface sediments of Svalbard, Arctic. Mar. Pollut. Bull. 184, 114116. https://doi.org/10.1016/j.marpolbul.2022.114116.

MacDonald, D.D., Ingersoll, C.G., Berger, T.A., 2000. Development and evaluation of consensus-based sediment quality guidelines for freshwater ecosystems. Arch. Environ. Contam. Toxicol. 39 (1), 20–31. https://doi.org/10.1007/s002440010075.

Marynowski, L., Czechowski, F., Simoneit, B.R.T., 2001. Phenylnaphthalenes and polyphenyls in palaeozoic source rocks of the holy cross mountains, Poland. Org. Geochem. 32 (1), 69–85. https://doi.org/10.1016/S0146-6380(00)00150-9.

Masclet, P., Mouvier, G., Nikolaou, K., 1986. Relative decay index and sources of polycyclic aromatic hydrocarbons. Atmos. Environ. 20 (3), 439–446. https://doi.org/10.1016/0004-6981(86)90083-1.

Masiá, A., Blasco, C., Picó, Y., 2014. Last trends in pesticide residue determination by liquid chromatography–mass spectrometry. Trends Environ. Anal. Chem. 2, 11–24. https://doi.org/10.1016/j.teac.2014.03.002.

Meyer, W., Seiler, T.-B., Schwarzbauer, J., Püttmann, W., Hollert, H., Achten, C., 2014. Polar polycyclic aromatic compounds from different coal types show varying mutagenic potential, EROD induction and bioavailability depending on coal rank. Sci. Total Environ. 320–328. https://doi.org/10.1016/j.scitotenv.2014.06.140.

Meyer zu Reckendorf, R., 2000. Phenyl-substituted polycyclic aromatic compounds as intermediate products during pyrolytic reactions involving coal tars, pitches and related materials. Chromatographia 52 (1), 67–76. https://doi.org/10.1007/BF02490795.

Moschet, C., Lew, B.M., Hasenbein, S., Anumol, T., Young, T.M., 2017. LC- and GC-QTOF-MS as complementary tools for a comprehensive micropollutant analysis in aquatic systems. Environ. Sci. Technol. 51 (3), 1553–1561. https://doi.org/10.1021/acs.est.6b05352.

Neale, P.A., Escher, B.I., de Baat, M.L., Dechesne, M., Dingemans, M.M.L., Enault, J., Pronk, G.J., Smeets, P.W.M.H., Leusch, F.D.L., 2023. Application of effect-based methods to water quality monitoring: answering frequently asked questions by water quality managers, regulators, and policy makers. Environ. Sci. Technol. 57 (15), 6023–6032.

Ngai, K.L., Plazek, D.J., 2002. Resolution of sub-rouse modes of polystyrene by dissolution. Macromolecules 35 (24), 9136–9141. https://doi.org/10.1021/acs.est.2c06365.

Ostojić, B.D., Stanković, B., Đorđević, D.S., 2014. Theoretical study of the molecular properties of dimethylanthracenes as properties for the prediction of their biodegradation and mutagenicity. Chemosphere 111, 144–150. https://doi.org/10.1016/j.chemosphere.2014.03.067.

Öztürk, M., Kolak, U., Duru, M.E., Harmandar, M., 2009. GC-MS analysis of the antioxidant active fractions of Micromeria juliana with anticholinesterase activity. Nat. Prod. Commun. 4 (9), 1271–1276. https://doi.org/10.1177/1934578X0900400923.

Paglia, E., 2020. A higher level of civilisation? The transformation of Ny-Ålesund from Arctic coalmining settlement in Svalbard to global environmental knowledge center at 79° North. Polar Rec. 56, e15. https://doi.org/10.1017/S0032247419000603.

Platt, K.L., Degenhardt, C., Grupe, S., Frank, H., Seidel, A., 2002. Microsomal activation of dibenzo[def,mno]chrysene (anthanthrene), a hexacyclic aromatic hydrocarbon without a bay-region, to mutagenic metabolites. Chem. Res. Toxicol. 15 (3), 332–342. https://doi.org/10.1021/tx010131t.

Pouch, A., Zaborska, A., Pazdro, K., 2017. Concentrations and origin of polychlorinated biphenyls (PCBs) and polycyclic aromatic hydrocarbons (PAHs) in sediments of western Spitsbergen fjords (Kongsfjorden, Hornsund, and Adventfjorden). Environ. Monit. Assess. 189, 1–20. https://doi.org/10.1007/s10661-017-5858-x.

Qishlaqi, A., Beiramali, F., 2019. Potential sources and health risk assessment .of polycyclic aromatic hydrocarbons in street dusts of Karaj urban area, northern Iran. J. Environ. Health Sci. Eng. 17 (2), 1029–1044. https://doi.org/10.1007/s40201-019-00417-3.

Qiu, S., Zhang, S., Fang, Y., Qiu, G., Yin, C., Reddy, R.G., Zhang, Q., Wen, L., 2019. Effects of poplar addition on tar formation during the co-pyrolysis of fat coal and poplar at high temperature. RSC Adv. 9 (48), 28053–28060. https://doi.org/10.1039/c9ra03938d.

Ra, K., Kim, J.-K., Hong, S.H., Yim, U.H., Shim, W.J., Lee, S.-Y., Kim, Y.-O., Lim, J., Kim, E.-S., Kim, K.-T., 2014. Assessment of pollution and ecological risk of heavy metals in the surface sediments of Ulsan Bay, Korea. Ocean Sci. J. 49 (3), 279–289. https://doi.org/10.1007/s12601-014-0028-3.

Russo, C., Ciajolo, A., Stanzione, F., Tregrossi, A., Oliano, M.M., Carpentieri, A., Apicella, B., 2019. Investigation on chemical and structural properties of coal- and petroleum-derived pitches and implications on physico-chemical properties (solubility, softening and coking). Fuel 245, 478–487. https://doi.org/10.1016/j.fuel.2019.02.040.

Schymanski, E.L., Jeon, J., Gulde, R., Fenner, K., Ruff, M., Singer, H.P., Hollender, J., 2014. Identifying small molecules via high resolution mass spectrometry: communicating confidence. Environ. Sci. Technol. 48, 2097–2098.

Sim, W., Choi, S., Lee, H.-J., Kim, K., Park, K., Oh, J.-E., 2022. Evaluation of sample preparation methods for suspect and non-target screening in water, sediment, and biota samples using gas chromatography coupled to high-resolution mass spectrometry. Sci. Total Environ. 849, 157835. https://doi.org/10.1016/j.scitotenv.2022.157835.

Steenhuisen, F., van den Heuvel-Greve, M., 2021. Exposure radius of a local coal mine in an Arctic coastal system; correlation between PAHs and mercury as a marker for a local mercury source. Environ. Monit. Assess. 193 (8), 499. https://doi.org/10.1007/s10661-021-09287-5.

Sun, Y., Qin, S., Zhao, C., Li, Y., Yu, H., Zhang, Y., 2013. Organic geochemistry of semianthracite from the gequan mine, xingtai coalfield, China. Int. J. Coal Geol. 116–117, 281–292. https://doi.org/10.1016/j.coal.2013.05.003.

Taylor, N.D., Bell, A.T., 1980. Effects of Lewis acid catalysts on the cleavage of aliphatic and aryl-aryl linkages in coal-related structures. Fuel 59 (7), 499–506. https://doi.org/10.1016/0016-2361(80)90177-5.

Vecchiato, M., Barbaro, E., Spolaor, A., Burgay, F., Barbante, C., Piazza, R., Gambaro, A., 2018. Fragrances and PAHs in snow and seawater of Ny-Ålesund (Svalbard): local and long-range contamination. Environ. Pollut. 242, 1740–1747. https://doi.org/10.1016/j.envpol.2018.07.095.

Vedani, A., Dobler, M., Hu, Z., Smieško, M., 2015. OpenVirtualToxLab—a platform for generating and exchanging in silico toxicity data. Toxicol. Lett. 232 (2), 519–532. https://doi.org/10.1016/j.toxlet.2014.09.004.

Xiao, H., Brinkmann, M., Thalmann, B., Schiwy, A., Große Brinkhaus, S., Achten, C., Eichbaum, K., Gembé, C., Seiler, T.-B., Hollert, H., 2017. Toward streamlined identification of dioxin-like compounds in environmental samples through integration of suspension bioassay. Environ. Sci. Technol. 51 (6), 3382–3390. https://doi.org/10.1021/acs.est.6b06003.

Yang, L., Li, M., Wang, T.G., Liu, X., Jiang, W., Fang, R., Lai, H., 2017. Phenyldibenzofurans and methyldibenzofurans in source rocks and crude oils, and their implications for maturity and depositional environment. Energy Fuels 31 (3), 2513–2523. https://doi.org/10.1021/acs.energyfuels.6b02801.

Yu, N., Guo, H., Yang, J., Jin, L., Wang, X., Shi, W., Zhang, X., Yu, H., Wei, S., 2018. Non-target and suspect screening of per- and polyfluoroalkyl substances in airborne particulate matter in China. Environ. Sci. Technol. 52 (15), 8205–8214. https://doi.org/10.1021/acs.est.8b02492.

Yunker, M.B., Macdonald, R.W., Ross, P.S., Johannessen, S.C., Dangerfield, N., 2015. Alkane and PAH provenance and potential bioavailability in coastal marine sediments subject to a gradient of anthropogenic sources in British Columbia, Canada. Org. Geochem. 89–90, 80–116. https://doi.org/10.1016/j.orggeochem.2015.10.002.

Yunker, M.B., Perreault, A., Lowe, C.J., 2012. Source apportionment of elevated PAH concentrations in sediments near deep marine outfalls in Esquimalt and Victoria, BC, Canada: is coal from an 1891 shipwreck the source? Org. Geochem. 46, 12–37. https://doi.org/10.1016/j.orggeochem.2012.01.006.

Zedda, M., Zwiener, C., 2012. Is nontarget screening of emerging contaminants by LC-HRMS successful? A plea for compound libraries and computer tools. Anal. Bioanal. Chem. 403 (9), 2493–2502. https://doi.org/10.1007/s00216-012-5893-y.

Zhao, Z., Gong, X., Zhang, L., Jin, M., Cai, Y., Wang, X., 2021. Riverine transport and water-sediment exchange of polycyclic aromatic hydrocarbons (PAHs) along the middle-lower Yangtze River, China. J. Hazard Mater. 403, 123973. https://doi.org/10.1016/j.jhazmat.2020.123973.

<Supplementary Materials>

Characterization of AhR-mediated potency in sediments from Kongsfjorden, Svalbard: Application of effect-directed analysis and nontarget screening

Jiyun Gwak [1], Jihyun Cha [1], Seung-Il Nam, Jung-Hyun Kim, Junghyun Lee,

Hyo-Bang Moon, Jong Seong Khim, Seongjin Hong [*]

This PDF file includes:

Number of pages: 21

Number of Supplementary Tables: 13, Tables S1 to S13

Number of Supplementary Figures: 3, Figs. S1 to S3

References

[1] These authors contributed equally to this work.

*** Corresponding Author.** *E-mail address*: hongseongjin@cnu.ac.kr (S. Hong).

Supplementary Tables

Table S1. Reverse phase (RP)-HPLC conditions for fractionation of silica gel column fractions (Hong et al., 2016).

Instrument	Agilent 1260 HPLC system (Preparative scale) 1260 Multiple wavelength detector
Column	PrepHT XDB-C18 reverse phase column (250 mm × 21.2 mm × 7 μm)
Mobile phase	A: Water, B: Methanol
Flow rate	10 mL min^{-1}
Injection volume	1 mL
Mobile phase gradient	40% A (0 min) → 40–0% A (0–40 min) → 0% A (40–60 min) → 0–40% A (60–62 min) → 40% A (62–70 min) 60% B (0 min) → 60–100% B (0–40 min) → 100% B (40–60 min) → 100–60% B (60–62 min) → 60% B (62–70 min)
Test standards	34 polychlorinated biphenyls 16 polycyclic aromatic hydrocarbons 7 alkylphenols 5 phthalates
Fractions collected times	

RP-HPLC Sub-fraction	Starting –End sampling time (min.)	Volume (mL)	Log K_{OW}
1	3.11 – 6.35	38	< 1
2	6.35 – 12.83	65	1 – 2
3	12.83 – 19.32	65	2 – 3
4	19.32 – 25.80	65	3 – 4
5	25.80 – 32.29	65	4 – 5
6	32.29 – 38.78	65	5 – 6
7	38.78 – 45.26	65	6 – 7
8	45.26 – 51.70	65	7 – 8
9	51.70 – 58.23	65	8 – 9
10	58.23 – 64.72	65	> 9

Table S2. Description of the experimental conditions for H4IIE-*luc* in vitro bioassay.

Bioassay procedure		**In vitro bioassays** **H4IIE-*luc***
Mode of action		AhR-mediated potencies
Culture condition	Temperature	37 °C
	Gas carrier	5% CO_2
	Culture flask	TC-treated culture dish
Seeding condition	Test Chamber	96-well plate
	Initial concentrations	7.0×10^4 cells mL^{-1}
	Volume	250 µL $well^{-1}$
	Incubation time	24 h
Dosing	Positive control	Benzo[*a*]pyrene (50, 17, 6.0, 2.0, 0.62, and 0.21 nM)
	Samples	Raw extracts, silica gel fractions, and RP-HPLC fractions
	Solvent control	0.1% DMSO
	Volume	250 µL $well^{-1}$
	Replicates	3
	Test duration	4 h
Ending	Endpoint	Luciferase activity
	Instrument	VictorX3 multilabel plate reader (PerkinElmer, Waltham, MA)

Table S3. Instrumental conditions of GC-MSD for analyses of PAHs (t-PAHs and e-PAHs), alkyl-PAHs, and SOs.

Instrument	GC: Agilent Technologies 7890B, MSD: Agilent Technologies 5977B	
Column	DB-5MS (30 m × 0.25 mm i.d. × 0.25 μm film)	
Carrier gas	Helium	
Flow rate	1.0 mL min^{-1}	
Injection volume	1.0 μL	
Mass range	50–600 *m/z*	
Ion source temperature	230 ℃	
Ionization mode	EI mode (70 eV)	
Oven temperature	PAHs and SOs	60 ℃ (hold 2 min) → 6 ℃ min^{-1} to 300 ℃ (hold 13 min)
	Alkyl-PAHs	60 ℃ (hold 2 min) → 6 ℃ min^{-1} to 162 ℃ (hold 0 min) → 2 ℃ min^{-1} to 168 ℃ (hold 0 min) → 6 ℃ min^{-1} to 300 ℃ (hold 13 min)

Table S4. Target compounds, abbreviations, target ions, and method detection limits in the GC-MSD analysis and recoveries of surrogate standards.

Target compounds	Abbreviation	Target ions		Method detection limit ($ng\ g^{-1}$ dw)
		Quantification ion	Confirmation ion	
Traditional PAHs (t-PAHs)				
Acenaphthene	Ace	153	154, 152	0.60
Acenaphthylene	Acl	152	151, 150	0.76
Fluorene	Flu	166	165, 167	0.65
Phenanthrene	Phe	178	176, 179	0.63
Anthracene	Ant	178	176, 179	0.70
Fluoranthene	Fl	202	200, 101	0.42
Pyrene	Py	202	200, 101	0.39
Benzo[*a*]anthracene	BaA	228	226, 229	0.27
Chrysene	Chr	228	226, 229	0.22
Benzo[*b*]fluoranthene	BbF	252	253, 250	0.19
Benzo[*k*]fluoranthene	BkF	252	253, 251	0.19
Benzo[*a*]pyrene	BaP	252	253, 126	0.17
Indeno[*1,2,3-cd*]pyrene	IcdP	276	138, 137	0.20
Dibenz[*a,h*]anthracene	DbahA	278	276, 279	0.33
Benzo[*g,h,i*]perylene	BghiP	276	138, 137	0.10
Emerging PAHs (e-PAHs)				
Benzo[*b*]naphtho[*2,3-d*]furan	BBNF	218	189, 219	0.34
11H-Benzo[*b*]fluorene	11BbF	216	215, 213	0.28
Benzo[*b*]naphtho[*2,1*-d]thiophene	BBNT	234	235, 232	0.17
5-Methylbenz[*a*]anthracene	5MBA	256	241, 239	0.11
Benzo[*j*]fluoranthene	BjF	252	253, 250	2.1
1-Methylchrysene	1MC	242	241	0.14
3-Methylchrysene	3MC	242	241	0.26
11H-benzo[*a*]fluorene	11BaF	216	215, 216	0.15
4,5-Methanochrysene	4,5MC	239	240, 241	0.10
Benz[*b*]anthracene	BbA	228	226, 229	0.32
7,12-dimethylbenz[*a*]anthracene	7,12DbA	256	241, 239	0.12
10-methylbenz[*a*]pyrene	10MbA	266	265, 263	0.12
7-methylbenz[*a*]anthracene	7MbA	242	241, 239	0.17
20-methylcholanthrene	20Mc	268	252, 253	0.30
Alkylated PAHs (alkyl-PAHs)				
1-Methylnaphthalene	1-Na	142	141	
2-Methylnaphthalene	2-Na	142	141	
1,3-Dimethylnaphthalene	1,3-Na	156	141	
1,4,5-Trimethylnaphthalene	1,4,5-Na	170	155	
1,2,5,6-Tetramethylnaphthalene	1,2,5,6-Na	184	169	
1-Methylfluorene	1-Flu	180	165	
9-Methylfluorene	9-Flu	180	165	
Dibenzothiophene	Dbthio	184	185	
2-Methyldibenzothiophene	2-Dbthio	198	197	
2,4-Dimethyldibenzothiophene	2,4-Dbthio	212	197	
2,4,7-Trimethyldibenzothiophene	2,4,7-Dbthio	226	211	
3-Methylphenanthrene	3-Phe	192	191	
2-Methylphenanthrene	2-Phe	192	191	
1,6-Dimethylphenanthrene	1,6-Phe	206	191	
1,2-Dimethylphenanthrene	1,2-Phe	206	191	
1,2,9-Trimethylphenanthrene	1,2,9-Phe	220	-	
1,2,6,9-Tetramethylphenanthrene	1,2,6,9-Phe	234	219	

3-Methylchrysene	3-Chr	242	239	
6-Ethylchrysene	6-Ethyl-Chr	256	241	
1,3,6-Trimethylchrysene	1,3,6-Chr	252	264	
Styrene oligomers (SOs)				
1,3-Diphenylpropane	SD1	92	196, 105	0.19
cis-1,2-Diphenylcyclobutane	SD2	104	208, 78	0.18
2,4-Diphenyl-1-butene	SD3	91	208, 104	0.89
trans-1,2-Diphenylcyclobutane	SD4	104	208, 78	0.11
2,4,6-Triphenyl-1-hexene	ST1	91	117, 194	0.63
1e-Phenyl-4e-(1-phenylethyl)-tetralin	ST2	91	129, 207	0.66
1a-Phenyl-4e-(1-phenylethyl)-tetralin	ST3	91	129, 207	0.31
1a-Phenyl-4a-(1-phenylethyl)-tetralin	ST4	91	129, 207	0.70
1e-Phenyl-4a-(1-phenylethyl)-tetralin	ST5	91	129, 207	0.41
1,3,5-Triphenylcyclohexane	ST6	117	104, 130	0.88
Surrogate standards	**Abbreviation**	**Quantification ion**	**Confirmation ion**	**Surrogate recovery (%, mean ± SD)**
Acenaphthene-d10	Ace-d10	164	162	67 ± 15
Phenanthrene-d10	Phe-d10	188	189	90 ± 10
Chrysene-d12	Chr-d12	240	236	105 ± 10

Table S5. Instrumental conditions of GC-QTOFMS for nontarget screening analysis.

Instrument	GC: Agilent Technologies 7890B
	QTOFMS: Agilent Technologies 7200
Samples	S2 (F2.4–F2.8)
Column	DB-5MS UI (30 m × 0.25 mm i.d. × 0.25 μm film)
Carrier gas	He
Flow rate	1.2 mL $min.^{-1}$
Injection volume	2 μL
Mass range	50–800 *m*/*z*
Ion source temperature	230 °C
Ionization mode	EI mode (70 eV)
Software	Qualitative analysis B.07.01
	MassHunter Quantitative analysis
	Unknown analysis
	NIST Library (ver. 2014)

Table S6. Molecular formula, molecular weight, and relative potency (ReP) values for AhR agonists reported previously.

Compounds	Molecular formula	Molecular weight	ReP values	References
Traditional PAHs				
Benz[*a*]anthracene	$C_{18}H_{12}$	228	3.2×10^{-1}	Kim et al. (2019)
Chrysene	$C_{18}H_{12}$	228	8.5×10^{-1}	
Benzo[*b*]fluoranthene	$C_{20}H_{12}$	252	5.0×10^{-1}	
Benzo[*k*]fluoranthene	$C_{20}H_{12}$	252	4.8×10^{-1}	
Benzo[*a*]pyrene	$C_{20}H_{12}$	252	1.0	
Indeno[*1,2,3-c,d*]pyrene	$C_{22}H_{12}$	276	5.8×10^{-1}	
Dibenz[*a,h*]anthracene	$C_{22}H_{14}$	278	6.6×10^{-1}	
Emerging PAHs				
Benzo[*b*]naphtho[*2,3-d*]furan	$C_{16}H_{10}O$	218	8.2×10^{-2}	Kim et al. (2019)
11H-Benzo[*b*]fluorene	$C_{17}H_{12}$	216	2.4×10^{-1}	
Benzo[*b*]naphtho[*2,1-d*]thiophene	$C_{16}H_{10}S$	234	3.6×10^{-2}	
3-Methylchrysene	$C_{19}H_{14}$	242	1.5	
5-Methylbenz[*a*]anthracene	$C_{19}H_{14}$	242	4.2×10^{-1}	
1-Methylchrysene	$C_{19}H_{14}$	242	6.0	
Benzo[*j*]fluoranthene	$C_{20}H_{12}$	252	1.7	
11H-Benzo[*a*]fluorene	$C_{17}H_{12}$	216	1.2	Cha et al. (2019)
Benz[*b*]anthracene	$C_{18}H_{12}$	228	11	
4,5-Methanochrysene	$C_{19}H_{12}$	234	1.0	
7,12-Dimethylbenz[*a*]anthracene	$C_{20}H_{16}$	256	2.0×10^{-1}	Gwak et al. (2022)
7-Methylbenz[*a*]anthracene	$C_{19}H_{14}$	242	1.4	
10-Methylbenzo[*a*]pyrene	$C_{18}H_{12}$	266	1.2	
20-Methylcholanthrene	$C_{21}H_{16}$	268	3.2	
Styrene Oligomers				
1,3-Diphenylpropane	$C_{15}H_{16}$	196	2.3×10^{-3}	Hong et al. (2016)
2,4-Diphenyl-1-butene	$C_{16}H_{16}$	208	3.0×10^{-4}	
1e-Phenyl-4e-(1-phenylethyl)-tetralin	$C_{24}H_{24}$	312	2.7×10^{-3}	

Table S7. Concentrations of t-PAHs, e-PAHs, alkyl-PAHs, and SOs in the sediments of Kongsfjorden.

Compounds	Sites									
	S1	**S2**	**S3**	**S4**	**S5**	**S6**	**S7**	**S8**	**S9**	**S10**
t-PAHs (ng g^{-1} dw)										
Acl	0.15	67	43	4.6	0.21	<LOD	<LOD	<LOD	<LOD	<LOD
Ace	<LOD[a]	130	82	7.5	0.49	0.29	<LOD	<LOD	<LOD	<LOD
Flu	0.92	180	110	17	1.2	0.83	1.8	0.94	0.82	1.1
Phe	4.8	800	790	77	4.8	2.1	9.4	2.6	2.9	3.0
Ant	0.24	200	88	8.3	<LOD	<LOD	<LOD	<LOD	<LOD	<LOD
Fl	0.96	150	120	12	0.87	0.98	1.68	0.64	0.92	0.90
Py	1.1	140	120	12	0.76	0.91	2.5	0.89	1.00	1.6
BaA	0.36	130	140	7.3	<LOD	<LOD	0.29	0.04	0.33	<LOD
Chr	0.53	100	130	7.2	0.37	<LOD	1.3	<LOD	<LOD	<LOD
BbF	0.89	79	91	6.7	3.4	0.65	1.3	0.21	0.46	0.30
BkF	<LOD	11	8.6	1.2	0.61	<LOD	0.25	<LOD	<LOD	<LOD
BaP	0.20	86	78	5.0	1.0	0.25	0.17	<LOD	<LOD	<LOD
IcdP	<LOD	14	19	1.4	1.3	0.20	<LOD	<LOD	<LOD	<LOD
DbahA	0.08	13	13	0.91	0.35	<LOD	<LOD	<LOD	<LOD	<LOD
BghiP	0.62	31	46	2.1	2.1	0.25	1.2	0.10	0.17	0.12
e-PAHs (ng g^{-1} dw)										
BBNF	0.38	130	140	7.2	0.35	<LOD	<LOD	<LOD	<LOD	<LOD
11BaF	0.53	34	130	29	0.64	<LOD	2.88	<LOD	<LOD	<LOD
11BbF	<LOD	130	110	6.4	0.40	<LOD	0.54	<LOD	<LOD	<LOD
BBNT	<LOD	310	80	2.5	<LOD	<LOD	0.50	<LOD	<LOD	<LOD
BbA	0.36	31	64	7.2	0.39	0.32	0.56	<LOD	0.32	<LOD
3MC	<LOD	110	96	5.4	<LOD	<LOD	<LOD	<LOD	<LOD	<LOD
5MBA	<LOD	44.	33	0.93	<LOD	<LOD	<LOD	<LOD	<LOD	<LOD
4,5MC	0.08	31	19	1.2	<LOD	<LOD	<LOD	<LOD	<LOD	<LOD
1MC	0.15	89	60	3.5	0.17	<LOD	0.48	<LOD	<LOD	<LOD
7MbA	0.01	8.8	7.7	0.5	<LOD	<LOD	<LOD	<LOD	<LOD	<LOD
BjF	<LOD	12	16	<LOD	<LOD	<LOD	<LOD	<LOD	<LOD	<LOD
7,12DbaA	0.14	69	49	3.0	0.13	<LOD	0.26	<LOD	<LOD	<LOD
alkyl-PAHs (ng g^{-1} dw)										
C1-Na	8.7	5000	2400	340	14	3.1	2.8	3.0	4.1	3.3
C2-Na	15	9800	6900	650	24	3.4	15	3.2	4.4	5.1
C3-Na	24	17000	10000	1000	0.31	3.0	56	2.7	4.0	4.4
C4-Na	1.4	1400	810	89	2.6	0.61	7.9	0.63	0.61	0.73
C1-Flu	3.0	750	490	51	4.0	2.3	11	2.4	2.4	3.0
C2-Flu	6.3	1200	820	84	7.6	5.0	22	5.0	4.7	5.8
C0-Dbthio	<LOD	150	290	22	<LOD	<LOD	1.8	<LOD	<LOD	<LOD
C1-Dbthio	2.3	1400	1200	110	2.8	0.8	12	0.87	0.87	1.2
C2-Dbthio	1.3	850	940	78	2.0	0.69	14	1.2	0.98	1.3
C3-Dbthio	<LOD	450	400	40	1.3	0.55	5.6	0.71	0.41	1.0
C1-Phe	7.2	3600	1900	310	7.2	1.1	36	1.4	1.2	1.8
C2-Phe	14	7900	4300	640	17	3.8	93	5.3	4.1	6.6
C3-Phe	27	420	3900	1000	24	11	150	13	10	17
C4-Phe	20	2000	4700	1600	31	5.8	183	8.1	5.5	8.7
C1-Chr	3.4	870	680	68	3.1	1.0	19	1.1	0.73	1.1
C2-Chr	16	6700	3200	520	16	4.6	53	5.4	4.4	6.9
C3-Chr	2.3	1600	830	130	4.1	0.72	12	0.86	0.73	0.18
SOs (ng g^{-1} dw)										
SD1	<LOD	16	26	1.9	<LOD	<LOD	0.19	<LOD	<LOD	<LOD
SD2	<LOD	2.2	2.4	<LOD	<LOD	<LOD	<LOD	<LOD	<LOD	<LOD
SD3	<LOD	58	11	2.5	1.1	<LOD	<LOD	1.2	<LOD	<LOD

SD4	1.0	2.8	3.2	1.2	1.0	0.90	0.64	0.90	0.91	0.97
ST1	<LOD	4.1	4.5	<LOD	<LOD	<LOD	<LOD	<LOD	<LOD	<LOD
ST2	<LOD	2.4	<LOD	<LOD	<LOD	<LOD	<LOD	<LOD	<LOD	<LOD
ST3	<LOD	1.9	10	0.67	0.32	<LOD	<LOD	<LOD	<LOD	<LOD
ST4	<LOD	10	15	<LOD	<LOD	<LOD	<LOD	<LOD	<LOD	<LOD
ST5	<LOD	1.2	1.8	<LOD	<LOD	<LOD	<LOD	<LOD	<LOD	<LOD
ST6	1.8	15	30	1.6	1.9	1.7	1.6	0.81	1.2	1.2

[a] <LOD: Limit of detection.

Table S8. Concentrations of t-PAHs, e-PAHs, and alkyl-PAHs in coals collected from sites S2-1, S3-1, and S4-1 in Kongsfjorden.

Compounds	Sites		
	S2-1	S3-1	S4-1
t-PAHs (ng g^{-1} dw)			
Acl	450	410	590
Ace	590	480	550
Flu	230	180	94
Phe	2800	2700	3000
Ant	770	79	100
Fl	610	360	390
Py	620	45	54
BaA	23	22	27
Chr	770	38	49
BbF	430	390	660
BkF	16	210	520
IcdP	21	19	10
DbahA	76	57	53
BghiP	13	13	24
e-PAHs (ng g^{-1} dw)			
BBNF	1500	1600	2000
11BaF	55	58	83
11BbF	380	310	470
BBNT	180	510	700
BbA	11000	330	13000
3MC	130	120	160
5MBA	880	720	930
4,5MC	280	230	280
1MC	320	270	610
7MbA	650	600	790
BjF	20	210	520
7,12DbaA	490	7900	17000
20Mc	34	24	37
10MbA	350	300	320
alkyl-PAHs (ng g^{-1} dw)			
C1-Na	15000	25000	38000
C2-Na	26000	4200	56000
C3-Na	45000	67000	89000
C4-Na	3700	5400	7200
C1-Flu	230	180	94
C2-Flu	1500	1000	990
C0-Dbthio	2900	4300	4500
C1-Dbthio	4100	6100	8300
C2-Dbthio	2800	4500	5500
C3-Dbthio	1900	2700	2400
C1-Phe	860	1200	900
C2-Phe	2800	79	100
C3-Phe	7400	11000	13000
C4-Phe	15000	1500	27000
C1-Chr	13000	21000	27000
C2-Chr	29000	46000	53000
C3-Chr	770	38	49
C1-Na	880	1500	1400
C2-Na	7200	10000	11000
C3-Na	1500	2100	2100

Tabel S9. PCA-MLR results for source apportionment of PAHs in sediments from Kongsfjorden.

Compounds	**PC1**	**PC2**	**PC3**
Acl	0.117	-0.4804	-0.7420
Ace	0.230	-0.3577	-0.5551
Flu	-0.619	1.318	-0.3035
Phe	2.882	1.388	1.541
Ant	0.8678	-0.8235	-0.9534
Fl	-0.6659	1.3546	-0.3848
Py	-0.9433	2.161	-0.7627
BaA	0.6792	-0.7468	-0.7933
Chr	0.5545	-0.7186	-0.5355
BbF	-1.170	-0.3928	2.442
BkF	-0.3676	-0.4237	-0.2194
BaP	-0.0091	-0.6645	0.0225
IcdP	-0.6429	-0.4969	0.4818
DbahA	-0.2930	-0.3674	-0.5087
BghiP	-0.6207	-0.7497	1.271
Estimated sources	Coal	Petroleum combustion	Coal combustion
Variance (%)	39	39	20

Table S10. Concentrations of target AhR agonists in the RP-HPLC subfractions of the sediments (F2.6−F2.8 of S2 and S3) from Kongsfjorden.

Compounds	Abb[a]	S2			S3		
		F2.6	F2.7	F2.8	F2.6	F2.7	F2.8
Traditional PAHs and SOs							
Benz[*a*]anthracene	BaA	130			130		
Chrysene	Chr	103			130		
1,3-Diphenylpropane	SD1	16			26		
2,4-Diphenyl-1-butene	SD3	58			11		
Benzo[*b*]fluoranthene	BbF		79			91	
Benzo[*k*]fluoranthene	BkF		11			8.6	
Benzo[*a*]pyrene	BaP		86			78	
Indeno[*1,2,3-c,d*]pyrene	IcdP		14			19	
Dibenz[*a,h*]anthracene	DahA		13			13	
2,4,6-Triphenyl-1-hexene	ST2		2.4			0.6	
Emerging PAHs							
Benzo[*b*]naphtho[*2,3-d*]furan	BBNF	130			140		
Benz[*b*]anthracene	BbA	31			64		
1-Methylchrysene	1MC		89			60	
3-Methylchrysene	3MC		110			96	
11H-Benzo[*b*]fluorine	11BbF		130			110	
Benzo[*b*]naphtho[*2,1-d*]thiophene	BBNT		310			80	
5-Methylbenz[*a*]anthracene	5MBA		44			33	
Benzo[*j*]fluoranthene	BjF		12			16	
11H-Benzo[*a*]fluorine	11BaF		34			130	
4,5-Methanochrysene	4,5MC		31			19	
10-Methylbenzo[*a*]pyrene	10MbA		8.2			6.3	
7,12-Dimethylbenz[*a*]anthracene	7,12DbA		69			49	
7-Methylbenz[*a*]anthracene	7MbA		8.8			7.7	
20-Methylcholanthrene	20Mc			7.3			5.6
Sum of concentrations of target AhR agonists		470	1050	7.3	510	820	5.6

[a] Abb: abbreviation.

[b] n.a: not available.

Table S11. Potency balance between instrument-derived BaP-EQs ($BaP\text{-}EQ_{chem}$) and bioassay-derived BaP-EQs ($BaP\text{-}EQ_{bio}$) in the RP-HPLC fractions of the sediments (F2.6−F2.8 of S2 and S3) from Kongsfjorden.

Compounds	**Abb**[a]	**S2**			**S3**		
		F2.6	**F2.7**	**F2.8**	**F2.6**	**F2.7**	**F2.8**
Instrument-derived BaP-EQs (ng BaP-EQs g^{-1} dw)							
Traditional PAHs and SOs							
Benz[*a*]anthracene	BaA	45			48		
Chrysene	Chr	97			120		
1,3-Diphenylpropane	SD1	0.047			0.078		
2,4-Diphenyl-1-butene	SD3	0.021			0.0041		
Benzo[*b*]fluoranthene	BbF		39			45	
Benzo[*k*]fluoranthene	BkF		5.4			4	
Benzo[*a*]pyrene	BaP		86			78	
Indeno[*1,2,3-c,d*]pyrene	IcdP		7.4			10	
Dibenz[*a,h*]anthracene	DahA		7.7			7.7	
2,4,6-Triphenyl-1-hexene	ST2		0.0052			0.0013	
Emerging PAHs							
Benzo[*b*]naphtho[*2,3-d*]furan	BBNF	13			12		
Benz[*b*]anthracene	BbA	360			750		
1-Methylchrysene	1MC		550			380	
3-Methylchrysene	3MC		170			150	
11H-Benzo[*b*]fluorine	11BbF		38			32	
Benzo[*b*]naphtho[*2,1-d*]thiophene	BBNT		12			3.1	
5-Methylbenz[*a*]anthracene	5MBA		19			14	
Benzo[*j*]fluoranthene	BjF		21			27	
11H-Benzo[*a*]fluorine	11BaF		32			20	
4,5-Methanochrysene	4,5MC		74			180	
10-Methylbenzo[*a*]pyrene	10MbA		10			7.4	
7,12-Dimethylbenz[*a*]anthracene	7,12DbA		13			9.2	
7-Methylbenz[*a*]anthracene	7MbA		13			12	
20-Methylcholanthrene	20MC			22			17
Total of instrument-derived BaP-EQs (ng BaP-EQ g^{-1} dw)		520	1100	22	930	980	17
Bioassay-derived BaP-EQs (ng BaP-EQs g^{-1} dw)		250	2100	480	110	4600	520
Contribution (%)		210	52	4.5	830	21	3.2

[a] Abb: abbreviation.
[b] n.a: not available.

Table S12. Toxic potentials of target AhR agonists in sediments predicted using VirtualToxLab (Cha et al., 2019; Gwak et al., 2022; Kim et al., 2019).

Compounds	Abbreviation	RePs	Toxic potential using VirtualToxLab modeling[a]
Benzo[*a*]anthracene	BaA	0.32	0.418
Chrysene	Chr	0.85	0.397
Benzo[*b*]fluoranthene	BbF	0.5	0.449
Benzo[*k*]fluoranthene	BkF	0.48	0.449
Benzo[*a*]pyrene	BaP	1	0.418
Indeno[*1,2,3-c,d*]pyrene	IcdP	0.58	0.442
Dibenz[*a,h*]anthracene	DbahA	0.66	0.474
Benzo[*b*]naphtho[*2,3-d*]furan	BBNF	0.082	0.411
11H-Benzo[*b*]fluorene	11BbF	0.24	0.401
Benzo[*b*]naphtho[*2,1-d*]thiophene	BBNT	0.036	0.367
1-Methylchrysene	1MC	6.0	0.404
3-Methylchrysene	3MC	1.5	0.400
Benzo[*j*]fluoranthene	BjF	1.7	0.436
5-Methylbenz[*a*]anthracene	5MBA	0.42	0.423
Benz[*b*]anthracene	BbA	10.6	0.422
11H-Benzo[*a*]fluorene	11BaF	1.2	0.394
4,5-Methanochrysene	4,5MC	1.0	0.384
10-Methylbenzo[*a*]pyrene	10MbA	1.2	0.398
7,12-Dimethylbenz[*a*]anthracene	7,12DbA	0.2	0.417
7-Methylbenz[*a*]anthracene	7MbA	1.4	0.405
20-Methylcholanthrene	20Mc	3.2	0.437

[a] 0.0−0.2: none binding, 0.2−0.4: low binding, 0.2−0.4: moderate binding, 0.4−0.6: elevated binding.

Table S13. Predicted potential toxic effects of tentative AhR agonists in sediments from Kongsfjorden using VEGA QSAR.

Compounds	AR activity[a]	ER activity[b]	GR Activity[c]	TR Activity[d]	Mutagenicity[e]	Developmental toxicity[f]	Carcinogenicity[g]
F2.4							
8-Methyl-2H-pyrano[*2,3-b*]quinoline	–[h]	– –	–	– –	+[i] – – –	+ –	+ – + +
F2.5				– –			
9-Ethyl-9,10-dihydroanthracene	–	– –	–	– –	– – – +	+ –	– – – +
1-Methylphenanthrene	+	– –	–	– –	+ + + +	+ –	+ + + +
3-Methylphenanthrene	+	– –	–	– –	+ + + +	+ –	+ ++ –
9,10-Dihydroanthracene	–	– –	–	– –	– – – –	+ –	– – – –
Phenylnaphthalene	+	– –	–	– –	– – – –	+ –	+ – + –
9,9-Dimethyl-9H-xanthen	–	– +	–	– –	– – – –	+ –	– – – +
F2.6							
1,7-Dimethylphenanthrene	+	–	–	– –	+ + + +	+ –	+ + + +
1-Methylphenanthro[*4,5-bcd*]thiophene	+	– +	–	– –	+ + + +	+ +	+ + + +
1-Methylpyrene	+	– +	–	– –	+ + + +	+ –	+ + + +
2,3,5-Trimethylphenanthrene	+	– +	–	– –	+ + + +	+ –	+ + + –
2,3-Dimethylphenanthrene	+	– –	–	– –	+ + + +	+ –	+ + + +
2,5-Dimethylphenanthrene	+	– –	–	– –	+ + + +	+ –	+ + + –
2,7-Dimethylanthracene	–	– +	–	– –	+ + + +	+ –	– – – +
2-Benzylnaphthalin	–	– –	–	– –	– – – +	+ –	– – + –
2-Phenyldibenzofuran	+	– +	–	– –	– + – +	+ –	+ + + +
3,6-Dimethylphenanthrene	+	– –	–	– –	+ + + +	+ –	+ + + –
4-Methylpyrene	+	– +	–	– –	+ + + +	+ –	+ + + +
4-Phenyldibenzofuran	+	– +	–	– –	– + – +	+ –	– + + +
9-Ethylanthracene	–	– –	–	– –	+ + + +	+ –	+ + + +
9-sec-Butyl-9,10-dihydroanthracen	–	– +	–	– –	– – – +	+ –	+ – – –
9-Vinylanthracene	–	– –	–	– –	+ + + +	+ –	+ + + +
1,2,3,4,5,6-Hexahydroanthracene	–	– –	–	– –	– – + +	+ –	– – – +
2-(4-Phenoxyphenoxy)ethyl benzoate	–	– +	–	– –	– – – –	– –	– – – +
2-(2-Methylphenyl)naphthalene	+	– –	–	– –	– – – –	+ –	+ – + –
4,5-Dimethylphenanthrene	+	– –	–	– –	+ + + +	+ –	+ + + +
5,12-Dihydrotetracene	–	– +	–	– –	+ + – +	+ –	+ + + –
6,13-Dihydrodibenzo[*b,i*]phenazine	–	– –	–	– –	+ + + +	+ –	+ + + +
9,10-Dimethylphenanthren	+	– –	–	– –	+ + + +	+ +	+ + + +
F2.7							
1,12-Dimethylbenzo[*c*]phenanthrene							
1-Methylbenzo[*c*]phenanthrene	+	– +	–	– –	+ + + +	+ –	+ + + +
2,3,6,7-Tetramethylanthracene	–	– +	–	– –	+ + + +	+ –	+ + + +

2,4,5,7-Tetramethylphenanthrene	+	−+	−	−−	++++	+−	++++
2-Isopropyl-10-methylphenanthrene	+	−+	−	−−	++++	+−	++++
2-Methyltriphenylene	+	−+	−	−−	++++	−−	++++
Benzo[*e*]pyrene	+	−+	−	−−	++++	−−	++++
Gossypol	−	−+	−	−−	++++	−−	++++
8-Isopropyl-1,3-dimethylphenanthrene	−	−+	−	−−	−++−	+−	−+++
Retene	+	−+	−	−−	+++−	+−	++++
Tri-m-tolyl phosphate	−	−+	−	−−	+++−	++	−+++
1,2'-Binaphthalene	+	−+	−	−−	+−−+	+−	++++
10,18-Bisnorabieta-8,11,13-triene	−	−+	−	−−	−−−−	+−	+−++
12-Ethyltetraphene	−	−+	−	−−	+++−	+−	++++
F2.8							
Anthanthrene	+	−+	−	−−	++++	+−	++++
Simonellite	−	−+	−	−−	−++	+−	+−++
Nordehydroabietane	−	−+	−	−−	−−−	+−	+−−+
3,3,7-trimethyl-2,4-dihydro-1H-chrysene	−	−+	−	−−	++++	+−	++++
10,18-Bisnorabieta-5,7,9(10),11,13-pentaene	−	−+	−	−−	−+++	+−	+−++

[a] Androgen receptor (AR) activity: IRFMN-CERAPA.
[b] Estrogen receptor (ER) activity: IRFMN-CERAPP and IRFMN.
[c] Glucocorticoid receptor (GR) activity model: Oberon.
[d] Thyroid disrupting receptor (TR) activity model: NRMEA(alpha) and NRMEA(beta).
[e] Mutagenicity model: CAESAR, ISS, SarPY-IRFMN , and KNN-Read-Across.
[f] Developmental toxicity model: CAESAR and PG.
[g] Carcinogenicity model: CAESAR, ISS, IRFMN-ISSCAN-CGX, and IRFMN-Antares.
[h] −: not active.
[i] +: active.

Supplementary Figures

Fig. S1. Photograph of the environments surrounding the sediment sampling sites (S1–S10) in Kongsfjorden, Svalbard.

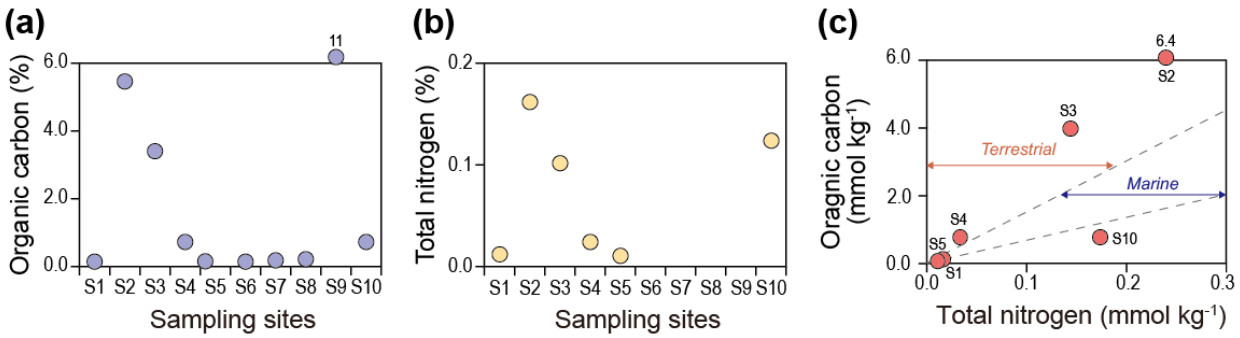

Fig. S2. (a) Organic carbon contents, **(b)** total nitrogen contents, and **(c)** C/N ratios in sediments from Kongsfjorden.

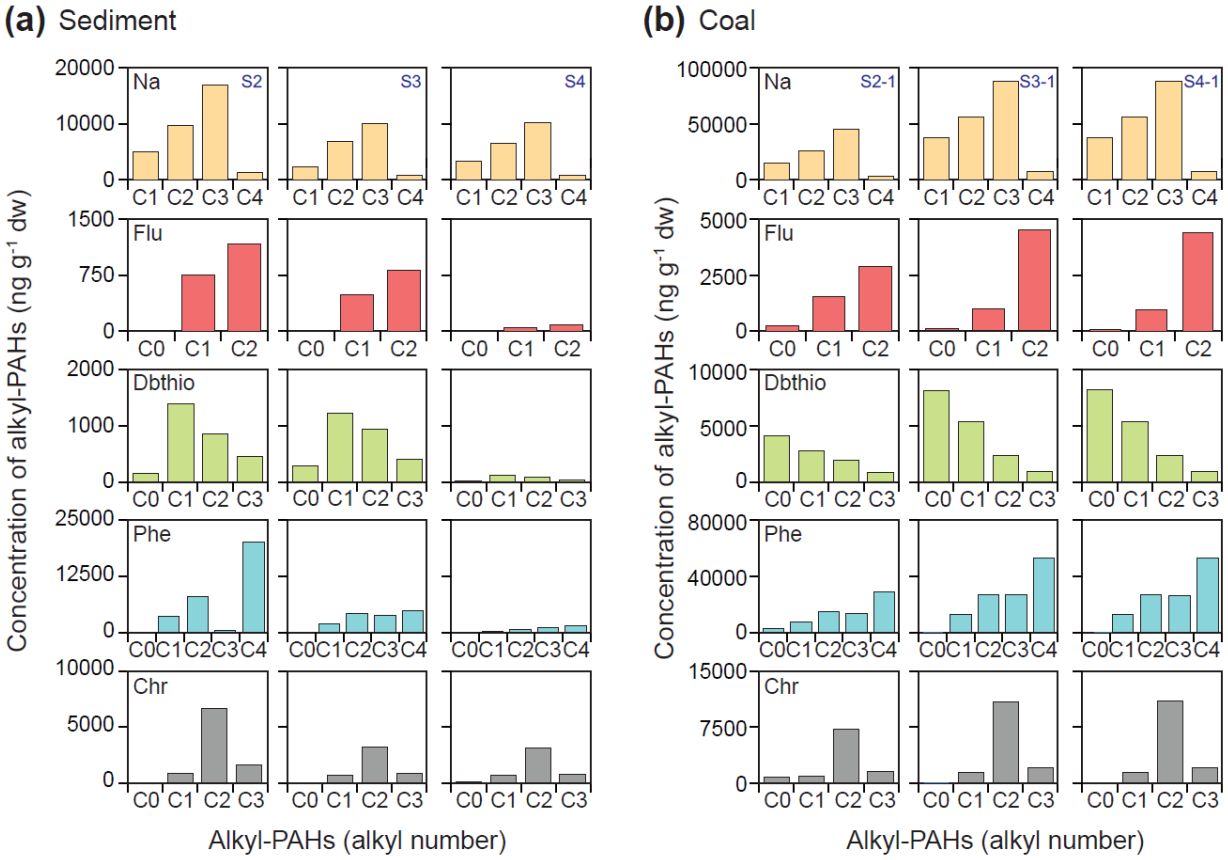

Fig. S3. Relative compositions of alkyl-PAHs in **(a)** sediments and **(b)** coals from Kongsfjorden.

References

Cha, J., Hong, S., Kim, J., Lee, J., Yoon, S.J., Lee, S., Moon, H.B., Shin, K.H., Hur, J., Giesy, J.P., Khim, J.S., 2019. Major AhR-active chemicals in sediments of Lake Sihwa, South Korea: application of effect-directed analysis combined with full-scan screening analysis. Environ. Int. 133, 105199. https://doi.org/10.1016/j.envint.2019.105199.

Gwak, J., Cha, J., Lee, J., Kim,Y., An, S.A., Lee, S., Moon, H.-B., Hur, J., Giesy, J.P, Hong, S., Khim, J.S., 2022. Effect-directed identification of novel aryl hydrocarbon receptor-active aromatic compounds in coastal sediments collected from a highly industrialized area. Sci. Total Environ. 803,149969. https://doi.org/10.1016/j.scitotenv.2021.149.

Hong, S., Lee, J., Lee, C., Yoon, S. J., Jeon, S., Kwon, B.O., Lee, J.H., Giesy, J.P., Khim, J.S., 2016. Are styrene oligomers in coastal sediments of an industrial area aryl hydrocarbon-receptor agonists? Environ. Pollut. 213, 913-921. https://doi.org/10.1016/j.envpol.2016.03.025.

Kim, J., Hong, S., Cha, J., Lee, J., Kim, T., Lee, S., Moon, H.B., Shin, K.H., Hur, J., Lee, J.S., Giesy, J.P., Khim, J.S., 2019. Newly identified AhR-active compounds in the sediments of an industrial area using effect-directed analysis. Environ. Sci. Technol. 53, 10043–10052. https://doi.org/10.1021/acs.est.9b02166.